1992

Stress Field Constraints on Intraplate Seismicity in Eastern North America

Mary Lou Zoback
U.S. Geological Survey, marylouz@stanford.edu

JOURNAL OF GEOPHYSICAL RESEARCH, VOL. 97, NO. B8, PAGES 11,761–11,782, JULY 30, 1992

Stress Field Constraints on Intraplate Seismicity in Eastern North America

MARY LOU ZOBACK

U.S. Geological Survey, Menlo Park, California

Focal mechanisms of 32 North American midplate earthquakes (m_b = 3.8–6.5) were evaluated to determine if slip is compatible with a broad-scale regional stress field derived from plate-driving forces and, if so, under what conditions (stress regime, pore pressure, and frictional coefficient). Using independent information on in situ stress orientations from well bore breakout and hydraulic fracturing data and assuming that the regional principal stresses are in approximately horizontal and vertical planes (±10°), the constraint that the slip vector represents the direction of maximum resolved shear stress on the fault plane was used to calculate relative stress magnitudes defined by the parameter $\phi = (S_2 - S_3)/(S_1 - S_3)$ from the fault/stress geometry. As long as the focal mechanism has a component of oblique slip (i.e., the B axis does not coincide with the intermediate principal stress direction), this calculation identifies which of the two nodal planes is a geometrically possible slip plane (Gephart, 1985). Slip in a majority of the earthquakes (25 of 32) was found to be geometrically compatible with reactivation of favorably oriented preexisting fault planes in response to the broad-scale uniform regional stress field. Slip in five events was clearly inconsistent with the regional stress field and appears to require a localized stress anomaly to explain the seismicity. Significantly, all five of these events occurred prior to 1970 (when many regional networks were installed), and their focal mechanisms are inconsistent with more recent solutions of nearby smaller events. The frictional likelihood of the geometrically possible slip on the selected fault planes was evaluated in the context of conventional frictional faulting theory. The ratio of shear to normal stress on the fault planes at hypocentral depth was calculated relative to an assumed regional stress field. Regional stress magnitudes were determined from (1) S_1/S_3 ratios based on the frictional strength of optimally oriented faults (the basis for the linear brittle portion of lithospheric strength profiles), (2) the computed relative stress magnitude (ϕ) values, and (3) a vertical principal stress assumed equal to the lithostat. Two end-member possibilities were examined to explain the observed slip in these less than optimally oriented fault planes. First, the frictional coefficient was held constant on all faults, hydrostatic pore pressure was assumed regionally, and the fault zone pore pressure was determined. Since pore pressure is a measurable quantity with real limits in the crust ($P_0 < S_3$), this end-member case was used to determine which of the geometrically possible slip planes were frictionally likely slip planes. Alternately, pore pressure was fixed at hydrostatic everywhere, and the required relative lowered frictional coefficient of the fault zone was computed. Slip in 23 of the 25 geometrically compatible earthquakes was determined to also be frictionally likely in response to an approximately horizontal and vertical regional stress field derived from plate-driving forces whose magnitudes are constrained by the frictional strength of optimally oriented faults (assuming hydrostatic pore pressure regionally). The conditions for slip on these 23 relatively "well-oriented" earthquake faults were determined relative to this regional crustal strength model and require only moderate increases in pore pressure (between about 0.4–0.8 of lithostatic, hydrostatic is about 0.37 of lithostatic) or, alternately, moderate lowering (<50%) of the frictional coefficient on the faults which slipped. Superlithostatic pore pressures are not required. Focal mechanisms for the two other earthquakes with slip vectors geometrically consistent with the regional stress field, however, did require pore pressures far exceeding the least principal stress (or extremely low coefficients of friction). These events may reflect either local stress rotations undetected with current sampling or poorly constrained focal mechanisms. The analysis also confirmed a roughly north to south contrast in stress regime between the central eastern United States and southeastern Canada previously inferred from a contrast in focal mechanisms between the two areas: most central eastern United States earthquakes occur in response to a strike-slip stress regime, whereas the southeastern Canadian events require a thrust faulting stress regime. This contrast in stress regime, with a constant maximum horizontal stress orientation determined by far-field plate-driving forces, requires a systematic lateral variation in relative stress magnitudes. Superposition of stresses due to simple flexural models of glacial rebound stresses are of the correct sense to explain the observed lateral variation, but maximum computed rebound-related stress magnitude changes are quite small (about 10 MPa) and do not appear large enough to account for the stress regime change if commonly assumed stress magnitudes determined from frictional strength apply to the crust at seismogenic depths.

INTRODUCTION

Unlike plate boundary earthquakes where forces driving deformation and seismically well-defined faults can be identified, intraplate seismicity represents diffuse deformation in relatively stable tectonic regions. Interestingly, data on the tectonic stress field suggests that many intraplate regions commonly have relatively consistent (±10°–15°) maximum horizontal stress orientations, midplate North America being perhaps the best and most well-sampled example [*Zoback et al.*, 1989; *Adams and Bell*, 1991; *Zoback and Zoback*, 1991]. The source of these broad-scale relatively uniform regional stress fields is believed to be primarily plate-driving forces [*Zoback et al.*, 1989, *Zoback*, this issue]. Independently derived stress data in intraplate regions can thus provide valuable constraints on the sources of intraplate seismicity and the conditions for slip in these events.

Paper number 92JB00221.

Two end-member hypotheses have been proposed to explain the occurrence of intraplate seismicity:

1. First is reactivation of preexisting faults in a uniformally oriented regional stress field with principal planes oriented approximately (±10°) horizontally and vertically. As the source of this relatively uniform broad-scale regional stress field is believed to be plate-driving forces, in intraplate setting this stress field should thus be relatively uniform and time-invariant. The preexisting faults may be selectively reactivated by local variations in pore pressure, fault friction, and/or strain localization along favorably oriented lower crustal ductile shear zones formed during earlier episodes of deformation [*Zoback et al.*, 1985*b*].

2. The second hypothesis is local stress perturbation. In this case the sense or orientation of slip recorded in intraplate events is incompatible with the regional stress field and is instead closely related to local stress anomalies such as lateral variations in crustal structure/density [e.g., *Goodacre and Hasegawa*, 1980; *Mareschal and Kuang*, 1986; *Richardson and Zoback*, 1990; *Zoback*, this issue], lithologic/strength contrasts [*Zoback et al.*, 1987], or stress concentrations along the edges of structures and bodies [e.g., *Kane*, 1977; *Hildebrand et al.*, 1977].

In this study these two hypotheses are evaluated for 32 well-constrained focal mechanisms of moderate North American intraplate earthquakes. (Note that the term intraplate is used herein to refer to the area of the North American plate east of the Rockies. This deformation is distinguished from active tectonism in the thermally elevated western U.S. Cordillera where deformation is dominated by Pacific-North American plate interactions.) Although it was not a selection criterion, all the events studied did exhibit oblique slip consistent with the idea (though not requiring it) that the earthquakes result from slip on preexisting fault planes which are reactivated in a stress field whose principal planes are approximately horizontal and vertical. New faults forming in such stress conditions would lie in the plane of the intermediate stress axis and exhibit either nearly pure dip-slip or strike-slip motion [*Anderson*, 1951]. A variety of data including the near verticality of dikes exposed over significant depth intervals, the observation of P, T, and B axes of focal mechanisms which are generally contained in planes within ±20° of horizontal and vertical, as well deep overcoring measurements of the complete stress tensor support the assumption that the principal planes of the regional stress field are approximately horizontal and vertical [e.g., *Zoback and Zoback*, 1980].

Most crustal earthquakes are believed to occur on preexisting faults [e.g., *Sibson*, 1989*b*; *Raleigh et al.*, 1972]; in this case the slip vector on the fault should coincide with the direction of maximum resolved shear stress on the fault plane [*Bott*, 1959]. The orientation of this shear stress depends on the orientation of the principal stresses relative to the fault plane as well as a linear relation between the stress magnitudes [after *Angelier*, 1979]:

$$\phi = (S_2 - S_3)/(S_1 - S_3) \quad (1)$$

This relationship provides constraints on the orientation of possible slip vectors and is independent of frictional resistance to sliding. In assessing the likelihood of slip in a given direction, the frictional strength of the preexisting fault must be evaluated; this requires information on stress magnitude and local pore pressure.

A two-step analysis methodology was developed to evaluate frictional reactivation of preexisting faults. First, independent information on the orientation of the regional stress tensor is used to calculate ϕ values from the fault/stress geometry for each set of nodal planes. This determines which planes are geometrically possible fault planes. In the second step, the shear and normal stresses acting on the selected planes are calculated using regional stress magnitudes determined from a model for stress differences based on the frictional strength of optimally oriented faults in a pervasively fractured crust, i.e., the linear brittle portion of the commonly used lithospheric strength profiles [e.g., *Sibson*, 1974; *Brace and Kolstedt*, 1980; *Zoback and Healy*, 1984]. The local pore pressure within the fault zone required to produce slip on the individual fault planes is calculated and used to determine which of the geometrically possible fault planes are frictionally likely fault planes.

The results of the analysis are used to categorize the style of faulting recorded in these intraplate earthquakes according to the two hypotheses given above. For the events which fall into the first category, slip on preexisting faults in response to the regional stress field, the analysis permits some definition of relatively "well-oriented" faults through limits placed on the local pore pressure conditions and/or the frictional strength of the faults associated with slip in these earthquakes.

STRESS DATA BASE FOR INTRAPLATE NORTH AMERICA

The contemporary tectonic stress data base for North America has been greatly improved over the last 10 years by the inclusion of a large amount of well bore breakout data and improved earthquake focal mechanisms. Determination of principal stress directions from stress-induced well bore breakouts utilizes the fact that the cross-sectional shape of many boreholes elongates in the direction of minimum horizontal compression due to the shear failure of the rock in the area of greatest compressive stress concentration around the borehole. This mechanism of formation of breakouts has been confirmed by theoretical [*Bell and Gough*, 1979; *Zoback et al.*, 1985*a*], laboratory [*Haimson and Herrick*, 1985; *Zheng et al.*, 1989], and field studies [*Hickman et al.*, 1985; *Stock et al.*, 1985; *Paillet and Kim*, 1988; *Shamir et al.*, 1988]. Consistency of breakout orientations within individual wells, between wells within a field, and with other nearby stress indicators indicates that breakouts are a very reliable measure of in situ stress orientation. Perhaps most significantly, however, breakout data from petroleum wells 2 to 4+ km deep fill a critical gap between the generally shallow (<1 km) in situ stress measurements and focal mechanisms for earthquakes which are typically in the 5–20 km depth range.

Figure 1 presents $S_{H\max}$ orientations for intraplate North America derived from the well bore breakout data as well as from earthquake focal mechanisms, hydraulic fracturing measurements, a few deep overcoring measurements made in mines in Canada, and geologic data from reverse faults with post-Miocene offsets within the U.S. Atlantic seaboard. The data indicate a remarkably uniform $S_{H\max}$ orientation throughout the intraplate region, varying between NE and east and averaging ENE, the Midplate Stress province (see *Zoback and Zoback* [1991] for a statistical analysis of stress directions in this region as well as a general discussion of

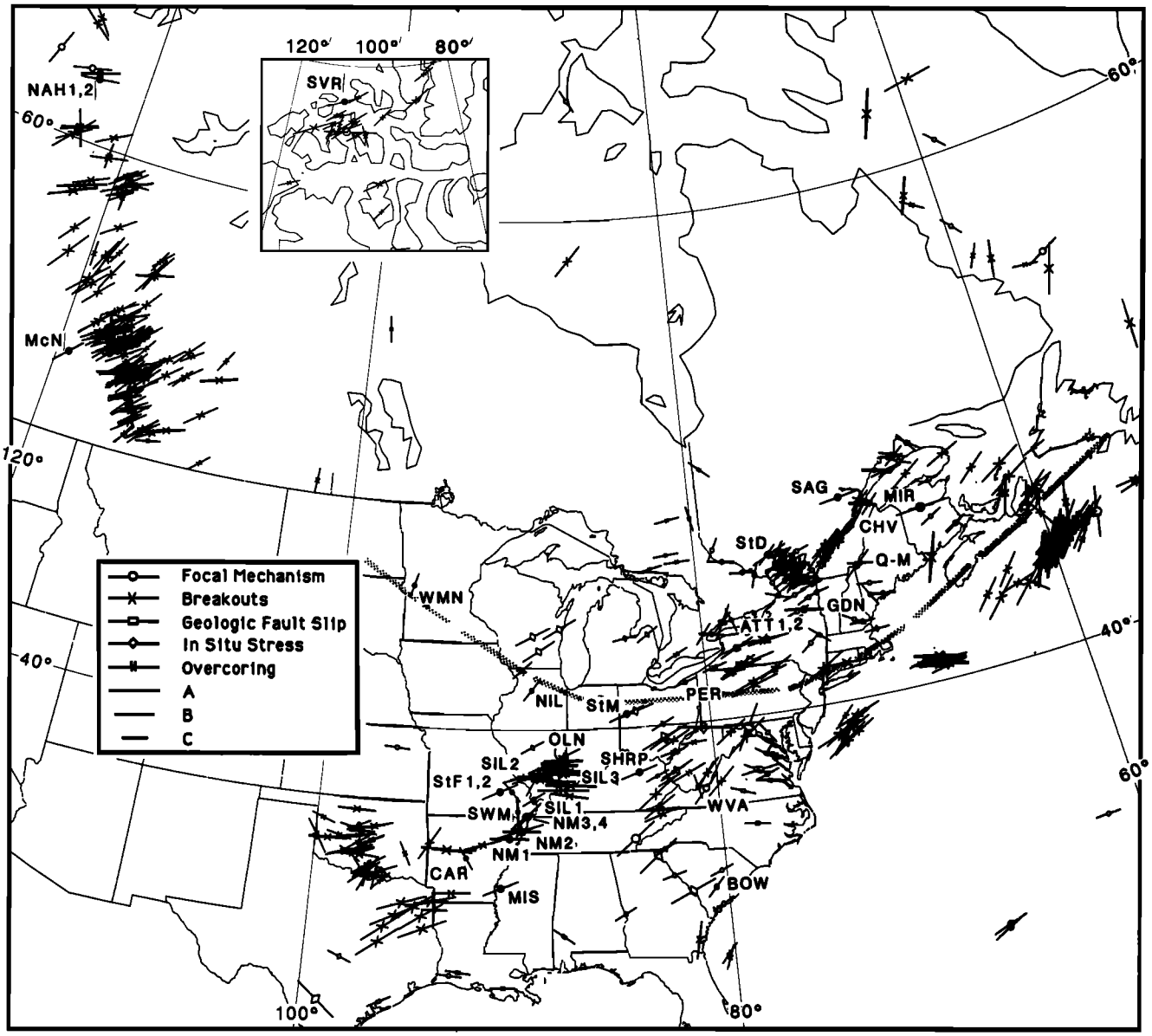

Fig. 1. Maximum horizontal stress orientations (S_{Hmax}) for midplate North America. Data lengths proportional to quality [*Zoback and Zoback*, 1989]; center symbol indicates type of stress indicator (see legend). Shaded heavy dashed line shows approximate southern limit of glacial warping [after *Barosh*, 1986]. Three and four letter codes (from Table 1) identifying earthquakes considered in the analysis described in the text are given next to the orientations of *P* axis for these events. Inset is a blowup of the Canadian Arctic region.

regional stress patterns throughout North America). The source of this uniform broad-scale regional stress field in midplate North America is believed to be related to plate-driving stresses [e.g., *Adams and Bell*, 1991; *Richardson and Reding*, 1991; *Zoback and Zoback*, 1991]. This orientation and its regional consistency were first noted by *Sbar and Sykes* [1973] in the northeast eastern United States and by *Haimson* [1977] in the Great Lakes region and by *Zoback and Zoback* [1980] for much of the central eastern United States. More recently, *Zoback et al.* [1986], *Hasegawa et al.*, [1985], *Adams* [1987, 1989], *Adams and Bell* [1991], and *Zoback and Zoback* [1989, 1991] have expanded the data coverage and the extent of the region characterized by this relatively uniform maximum horizontal stress direction to include most of the United States east of the Rockies and nearly all of Canada.

The data in Figure 1 are quality-ranked (indicated by the length of the orientation line) using the criteria of *Zoback and Zoback* [1989] (see also *Zoback and Zoback* [1991] and *Zoback* [this issue]). This quality is based on the accuracy of the measurements and the depth or depth interval sampled, as well as on the reliability of the technique as a tectonic stress indicator. Depths sampled range from surface fault offsets, near-surface in situ stress measurements (few hundred meters to 1–2 km), to 20–25 km depths for some of the deepest intraplate earthquakes. Of the 734 stress orientations shown on this map, 491 are from well bore breakouts.

The stress data shown in Figure 1 come from a variety of sources. A useful discussion and summary of most of the hydrofracture data for the north central United States are given by *Haimson and Doe* [1984]. Breakout data shown on

the map include data from *Plumb and Cox* [1987] for a large regional study covering northeastern United States and southernmost Canada, *Dart* [1985] for the Illinois basin, *Podrouzek and Bell* [1985] for the Scotian shelf, *Dart and Zoback* [1987] for the Atlantic outer continental margin, and *Dart* [1987] for the south central United States. The geologic fault offset data in the eastern United States are from the compilation of *Prowell* [1983]. Earthquake focal mechanism data come from a variety of sources, the focal mechanisms used in this study are discussed below, and references are given in Table 1. The Canadian data have been tabulated in detail by *Adams* [1987] and are most recently summarized by *Adams and Bell* [1991]. The U.S. data plotted on Figure 1 are discussed by *Zoback and Zoback* [1989] and *Zoback and Zoback* [1991]. Most of the data shown on Figure 1 are available on the CD-ROM "Geophysics of North America" distributed by the National Geophysical Data Center (NGDC), Boulder, Colorado. The entire data set shown in Figure 1 is included on the World Stress Map data base released as a companion to this special section of the *Journal of Geophysical Research* and being distributed by NGDC on floppy diskettes.

EARTHQUAKE DATA BASE FOR NORTH AMERICA

A number of moderate-size ($m_b \approx 4.0$–6.5) earthquakes have occurred in intraplate North America in the last 25 years. Thirty-two of these earthquakes were selected for analysis because they are the largest recent events and were judged to have the best constrained focal mechanisms. Many of the solutions (particularly those in the United States) come from studies by *Herrmann* [1973, 1979], *Herrmann and Canas* [1978], *Herrmann et al.* [1982], and *Nguyen and Herrmann* [1992] in which the mechanisms were determined using both first motions and forward modeling of surface waves. (All A and B quality solutions were used from *Herrmann*'s [1979] compilation with the exception of one "A" quality event on October 2, 1971, in Hudson Bay for which he determined a normal fault solution. A surface wave study of the same event by *Hashizume* [1974] indicated a reverse faulting solution.)

Information on each event is given in Table 1, including the focal mechanism (expressed as P and T axes and also strike, dip, and rake of each nodal plane using the Aki-Richards convention). The three- or four-letter identification codes listed in Table 1 are used throughout the text and on the figures to distinguish individual events. Note that two mechanisms are given for the Quebec-Maine event of June 15, 1973. The solution by *Herrmann* [1979], Q-MH, was based on limited first motions and surface wave modeling and had one shallowly dipping (23°) primarily strike-slip plane and a second very steeply dipping (80°) primarily thrust plane. The solution by *Yang and Aggarwaal* [1981], Q-MY, utilized more first-motion data and defined two moderately dipping planes, both with reverse oblique slip. An initial, preliminary solution for this event by *Wetmiller* [1975] actually indicated normal faulting, emphasizing the difficulty in constraining focal mechanisms for moderate intraplate events in regions with relatively sparse network coverage. To investigate the potential uncertainties in resolution of the focal mechanisms, both of the better constrained oblique reverse mechanisms for this event were considered in the analysis below.

The earthquakes studied are primarily from the central eastern United States and southeastern Canada. However, two of the events occurred in the Northwest Territories (NAH1, NAH2), one in eastern British Columbia (McN) and one in the Canadian Arctic islands (SVR); all of these areas are included in the "midplate North America" stress province based on the orientation of nearby breakout data [*Zoback et al.*, 1986; *Bell and Babcock*, 1986; *Adams and Bell*, 1991; *Zoback and Zoback*, 1989, 1991]. The three or four letter codes from Table 1 identify the $S_{H\max}$ orientations on Figure 1 inferred from P axis orientations for the earthquakes included in this study. Note that in the vicinity of these intraplate events, independent breakout and in situ stress data provide information on principal stress orientations.

The earthquakes selected for analysis listed in Table 1 are arranged by latitude to help evaluate regional variations in deformational style and possible variations in the stress field due to glacial rebound. Focal mechanisms for all the events in Table 1 are plotted in Figure 2; however in this figure the events are separated regionally into U.S. and Canadian subsets and are arranged by depth within each subset. All events have $m_b \geq 3.8$. The U.S. earthquakes range in magnitude from 3.8 to 5.5 and in depth from 1.5 to 22.0 km. The Canadian events range in magnitude from 4.1 to 6.5 and in depth from 6.0 to 29.0 km. As noted by *Hasegawa et al.* [1985] and *Talwani and Rajendran* [1991], there appear to be two different styles of deformation coinciding generally with a roughly north/south or Canada/U.S. regional separation: the U.S. events are primarily strike slip, whereas the Canadian events are primarily thrust faulting events.

Figure 3 is a lower hemisphere stereoplot of the P and T axes of the selected events, again the Canadian and U.S. events are distinguished. The near-horizontal P axes average ENE, consistent with the $S_{H\max}$ orientation for midplate North America inferred from other types of stress data. The orthogonal girdle of T axes lying in a NNW striking plane (with plunges ranging from horizontal to vertical) indicates compressional deformation characterized by either strike-slip or thrust faulting. The only exceptions to the regional compressive stress regime are the two normal faulting events (StF1 and StF2, Table 1) in the St. Francois Mountains, Missouri [*Mitchell*, 1973; *Patton*, 1976; *Herrmann*, 1979], which have T axes nearly orthogonal to one another, these two earthquakes clearly represent a localized stress anomaly. Three other exceptions to the ENE P axes trend can be seen in the stereoplot of P and T axes in Figure 3: one event in southwestern Missouri (SWM), one in central Arkansas (CAR), and one on the Virginia–West Virginia border (WVA). The anomalous P axes orientations of these events relative to the surrounding available stress data are also obvious on the stress map in Figure 1.

The contrast in faulting style between the Canadian and U.S. events obvious in the beachball plots in Figure 2 is also indicated by the variation in plunge of the T axes shown in Figure 3. The Canadian earthquakes are generally thrust events with steeply dipping T axes, whereas most of the U.S. events show oblique strike-slip movement with subhorizontal T axes. The beachball plots in Figure 2 sorted by depth do not indicate any clear depth variation in focal mechanisms for these largest earthquakes within the two geographic regions. Thus the contrast between the Canadian and the U.S. focal mechanisms may be best viewed as a N-S

variation in faulting style: a northern, predominately thrust group, and a southern, predominantly strike-slip group, with a separation at about latitude 41°–42°, as first noted by *Hasegawa et al.* [1985]. Events ATT1 and ATT2 near the Canadian–U.S. border region at about 42° show about equal components of dip-slip and strike-slip movement and may represent a transition between the two deformational styles. There are two obvious exceptions to the northern/thrust–southern/strike-slip categorization: the strike-slip earthquake in the Sverdrup Basin, located far north (76.8°N latitude) in the Canadian Arctic (SVR), and the deepest U.S. event (SIL3), a thrust earthquake in the southern Illinois basin.

FRICTIONAL FAULTING ANALYSIS OF THE FOCAL MECHANISMS

Geometric Constraints

The first step in critically evaluating slip in these events was to review the independent stress data available in the vicinity of each of the earthquakes and to determine a mean $S_{H\max}$ direction. This regional average $S_{H\max}$ direction in the vicinity of the individual events varied from N50°E to N85°E, depending on location (Table 1). There is typically a ±10° uncertainty in this average orientation.

A principal stress tensor was defined using the regional average $S_{H\max}$ orientations in the vicinity of the individual events and initially assuming that all principal stresses lie in horizontal and vertical planes. Both a thrust regime and a strike-slip regime were used to evaluate all events. The inferred principal stress field was resolved onto each of the nodal planes using a tensor transformation. The observed slip vector was equated with the orientation of maximum resolved shear stress on that fault plane and the corresponding ϕ value was calculated directly from the geometry of the fault plane and stress tensor using the expression (following *Gephart* [1985]):

$$\phi = -\frac{(\hat{n} \cdot \sigma_1)(\hat{b} \cdot \sigma_1)}{(\hat{n} \cdot \sigma_2)(\hat{b} \cdot \sigma_2)} \tag{2}$$

where $\hat{n}$ is a unit vector perpendicular to the fault plane, $\hat{b}$ is a unit vector perpendicular to n and to the slip vector, and σ_1 and σ_2 are unit vectors in the directions of the maximum and intermediate principal stress axes, respectively. It is important to note that for any given fault plane orientation there are three possible ϕ values, one for each of the stress regimes (normal, strike slip, and thrust) as the principal stresses σ_1, σ_2, and σ_3 assume different stress axes (horizontal and vertical) in the different regimes. (Note also that *Gephart* [1985] defined the relative stress magnitude ratio slightly differently; in his equation (3) he solved for R, where $R = 1 - \phi$. His equations (1) and (2) were rearranged to yield equation (2) above).

Gephart [1985] also demonstrated theoretically that unless the B axis coincides exactly with the intermediate stress axes, only one of the two possible slip planes (nodal planes) would have a permissible slip vector (ϕ value within the required range of $0 < \phi < 1$) for a given stress direction and stress regime. Thus this geometric constraint selects which one of the two nodal planes has slip geometrically compatible with the assumed regional stress field. In fact, a comparison of these selected "fault" planes with independently determined fault planes (e.g., by aftershock distribution) can provide a test of the assumption that the causative stress field has principal planes oriented approximately horizontally and vertically.

For the focal mechanisms used in this analysis, the authors typically assign a ±10° uncertainty to the focal parameters (strike, dip, and rake) [e.g., *Herrmann*, 1979]. To assess the significance of the uncertainties in focal slip parameters and in $S_{H\max}$ orientation, ϕ values were calculated for each nodal plane over a range of uncertainty in the orientation of the regional stress tensor. Three cases were considered, the first of these, the horizontal case, corresponds to a stress tensor with principal planes oriented strictly vertically and horizontally and with a ±10° range in possible $S_{H\max}$ orientation (corresponding to a rotation of the horizontal principal plane about a vertical axis). However, it is also possible that the principal stress directions in the Earth's crust do not lie strictly in true horizontal and vertical planes. To partially evaluate this effect, principal planes were also allowed to rotate 10° out of true horizontal and vertical orientations. Because there are an infinite number of possibilities for stress tensor orientations once true horizontal and vertical planes are abandoned, this effect was evaluated with two simple cases: In case 1, S_3 is held horizontal and S_1 and S_2 are rotated 10° from horizontal and vertical in the plane perpendicular to S_3, and in case 2, S_1 is held horizontal and S_2 and S_3 were rotated 10° from horizontal and vertical. The three cases correspond to stress states in which the principal axes are given in Table 2. These three cases represent the full range of uncertainties considered in this study; note that since the horizontal case has three possible stress tensor orientations (corresponding to $S_{H\max} \pm 10°$), a total of 10 possible stress configurations (five tensor configurations in each of the two regimes) were evaluated for each fault plane.

Frictional Constraints

The ϕ calculation described above determined which of the two nodal planes was a geometrically possible fault plane; thus the earthquake focal mechanism data set with two nodal planes for each event was reduced to a data set of possible fault planes and their associated slip vectors. To quantitatively assess the frictional likelihood of slip on these faults, the ratio of the shear stress acting in the direction of slip to the normal stress acting on the fault plane must be determined. Theoretical and laboratory studies indicate a linear law for frictional sliding:

$$\tau = C_0 + \mu(S_n - P_0) \tag{3}$$

where τ is the shear stress acting along the slip direction, C_0 is cohesive strength, μ is the coefficient of frictional sliding, S_n is the normal stress acting on the fault plane, and P_0 is the pore pressure. For slip on preexisting faults the cohesive strength, C_0 is commonly taken to be close to zero [*Brace and Kohlstedt*, 1980; *Zoback and Healy*, 1984] and (3) reduces to

$$\tau = \mu(S_n - P_0) \tag{4}$$

Determination of τ and S_n for each fault is done by tensor transformation and requires knowledge of the absolute magnitudes of the stresses (or magnitudes relative to one stress component since we are interested in a ratio of stresses).

Unfortunately, in situ measurements of stress magnitude

TABLE 1. Data for Earthquakes

Event	Date	Location	Latitude, °N	Longitude, °W	Depth, km	Azimuth/Plunge, deg		S_{Hmax} (N °E)
						P Axis	*T* Axis	
SVR	Dec. 27, 1972	Canada, Sverdrup Basin	76.80	106.49	20.0	65/05	335/05	65
NAH1	Oct. 5, 1985	Canada, Nahanni 1	62.24	124.27	6.5	67/14	215/73	60
NAH2	Dec. 23, 1985	Canada, Nahanni 2	62.22	124.24	6.0	84/25	252/65	60
McN	July 5, 1986	Canada, McNaughton Lake	52.65	118.89	12.0	41/18	158/59	55
SAG	Nov. 25, 1988	Canada, Saguenay	48.117	71.18	29.0	81/15	192/54	60
CHV	Aug. 19, 1979	Canada, Charlevoix	47.67	69.90	10.0	106/20	356/44	60
MIR	Jan. 9, 1982	Canada, Miramachi	47.00	66.60	7.0	264/01	172/67	65
StD	Feb. 18, 1978	Canada, St. Donat	46.30	74.10	7.0	250/04	40/81	55
WMN	July 9, 1975	Minnesota, western	45.70	96.00	7.5	17/14	283/14	50
Q-MH	June 15, 1973	Quebec-Maine, Herrmann	45.30	70.90	6.0	47/32	187/15	60
Q-MY	June 15, 1973	Quebec-Maine, Yang	45.30	70.90	6.0	257/01	352/64	60
GDN	Oct. 7, 1983	New York, Goodnow	43.94	74.26	7.5	277/15	68/73	70
ATT2	June 13, 1967	New York, Attica	42.90	78.2	3.0	74/11	336/53	70
ATT1	Jan. 1, 1966	New York, Attica	42.80	78.2	2.0	62/01	331/28	70
PER	Jan. 31, 1986	Ohio, Perry	41.65	81.16	7.0	75/07	342/21	70
NIL	Sept. 15, 1972	Illionis, platform	41.60	89.40	13.0	38/01	129/28	55
StM	July 12, 1986	Ohio, St. Mary	40.55	84.39	5.0	244/14	334/00	75
OLM	June 10, 1987	Illionis, Olney	38.71	87.95	10.0	89/04	357/24	75
SIL2	April 3, 1974	Illionis, Illinois basin	38.60	88.10	15.0	267/14	173/14	75
SHRP	July 27, 1980	Kentucky, Sharpsburg	38.17	83.91	18.0	251/21	349/21	65
SIL3	Nov. 9, 1968	Illinois, Illinois basin	38.00	88.50	22.0	97/01	192/82	75
StF1	Oct. 21, 1965	Missouri, St. Francois Mountains	37.50	91.00	5.0	273/76	156/07	75
StF2	July 21, 1967	Missouri, St. Francois Mountains	37.50	90.40	15.0	314/52	50/05	75
WVA	Nov. 20, 1969	West Virginia/Virginia border	37.4	81.00	5.0	166/00	256/14	60
SIL1	Aug. 14, 1965	Illinois, Illinois Basin	37.20	89.30	1.5	239/28	148/01	80
SWM	March 3, 1963	Missouri, southwest	36.70	90.10	15.0	174/11	77/31	75
NM4	Feb. 2, 1962	Missouri, NW rift margin	36.50	89.60	7.5	43/19	301/28	75
NM3	June 13, 1975	Missouri, NW rift margin	36.50	89.70	9.0	49/34	313/08	75
NM2	Nov. 17, 1970	Arizona, rift axis	35.90	89.90	16.0	272/09	176/32	75
NM1	March 25, 1976	Arizona, rift axis	35.60	90.50	12.0	272/01	181/38	75
CAR	Jan. 1, 1969	Arizona, central	34.80	92.60	7.0	329/06	227/65	80
MIS	June 4, 1967	Mississippi, western	33.60	90.90	12.0	248/07	155/21	70
BOW	Feb. 3, 1972	South Carolina, Bowman	33.31	80.58	2.0	221/28	107/38	55

*Centered dot indicates slip geometrically impossible for the assumed regional stress tensor orientation; a plus indicates slip geometrically possible but frictionally unlikely (using constraint that pore pressure must be less than S_3) for the assumed regonal stress tensor orientation; and a cross indicates slip geometrically possible and frictionally likely (using constraint that pore pressure must be less than S_3) for the assumed regonal stress tensor orientation.

Used in Study

m_b	Nodal Planes: Strike (N°E)	Nodal Planes: Dip, deg	Nodal Planes: Rake, deg	Thrust Regime*: Horizontal: S_{Hmax}	Thrust Regime*: Horizontal: +10°	Thrust Regime*: Horizontal: −10°	Thrust Regime*: 1	Thrust Regime*: 2	Strike-Slip Regime*: Horizontal: S_{Hmax}	Strike-Slip Regime*: Horizontal: +10°	Strike-Slip Regime*: Horizontal: −10°	Strike-Slip Regime*: 1	Strike-Slip Regime*: 2	Reference†
5.7	110	83	0	·	·	·	·	+	X	X	X	·	X	3
	20	90	173	·	·	·	·	·	·	·	·	X	·	
6.5	169	32	107	X	X	·	X	·	·	·	+	·	·	1
	330	60	80	·	·	+	·	·	·	·	·	+	·	
6.4	184	21	103	X	X	X	X	·	·	·	·	·	·	1
	350	70	85	·	·	·	·	·	·	·	·	·	·	
4.8	164	36	138	·	·	·	·	+	+	X	+	+	+	14
	290	67	62	+	+	+	+	·	·	·	·	·	·	
5.9	207	41	144	X	X	X	X	·	·	·	·	·	·	13
	326	67	55	·	·	·	·	X	+	·	+	+	+	
5.0	152	43	22	·	·	·	·	+	+	·	+	·	+	2
	46	76	131	+	+	+	+	·	·	·	·	·	·	
5.7	332	49	59	·	·	·	·	·	+	·	+	+	+	17
	195	50	121	X	X	X	X	X	·	·	·	·	·	
4.1	345	39	97	X	X	X	X	·	·	·	·	·	·	11
	156	51	84	·	·	·	·	·	·	·	+	·	·	
4.6	60	70	0	·	·	·	X	X	X	X	·	·	X	6
	150	90	−160	·	·	·	·	·	·	·	·	+	·	
5.0	185	23	153	·	·	·	+	·	+	X	+	+	+	6
	300	80	70	+	+	+	·	X	·	·	·	·	·	
5.0	11	49	125	X	X	X	X	·	+	·	+	+	+	18
	144	52	56	·	·	·	·	X	·	·	·	·	·	
5.1	342	31	106	X	X	X	X	X	·	·	·	·	·	12
	180	60	81	·	·	·	·	·	·	·	·	·	·	
4.4	130	47	37	·	·	·	·	X	X	+	X	X	X	5
	13	64	131	+	+	+	+	·	·	·	·	·	·	
4.6	110	70	20	X	·	X	X	·	·	X	·	·	·	5
	13	71	159	·	X	·	·	+	X	·	+	+	X	
5.0	115	71	10	·	·	·	X	+	X	X	X	·	X	10
	22	81	161	+	+	+	·	·	·	·	·	X	·	
4.4	170	70	160	·	·	·	X	+	+	X	+	·	+	6
	267	71	21	X	X	X	·	·	·	·	·	X	·	
4.5	288	80	10	·	·	·	·	+	X	X	X	X	X	15
	20	80	−170	·	·	·	·	·	·	·	·	·	·	
4.9	136	70	15	·	·	·	X	+	X	+	X	·	X	16
	41	76	160	X	X	X	·	·	·	·	·	X	·	
4.7	310	70	0	·	·	·	·	+	X	X	X	X	X	6
	220	90	160	·	·	·	·	·	·	·	·	·	·	
5.2	30	60	180	·	·	·	·	X	X	X	X	X	X	9
	300	90	−30	·	·	·	·	·	·	·	·	·	·	
5.5	195	45	101	X	X	·	X	·	X	X	·	X	·	4
	359	46	79	·	·	·	·	·	·	·	·	·	·	
4.9	260	40	−71	·	·	·	·	·	·	·	·	·	·	6
	55	53	−106	·	·	·	·	·	·	·	·	·	·	
4.3	107	52	−141	·	·	·	·	·	·	·	·	·	·	6
	350	60	−45	·	·	·	·	·	·	·	·	·	·	
4.6	32	80	10	·	·	·	·	·	·	·	·	·	·	6
	300	80	170	·	·	·	·	·	·	·	·	·	·	
3.8	280	70	−20	·	·	·	·	X	X	X	X	X	X	6
	17	71	−159	·	·	·	·	·	·	·	·	·	·	
4.8	220	60	15	·	·	·	·	·	·	·	·	·	·	6
	122	77	149	·	·	·	·	·	·	·	·	·	·	
4.3	84	55	7	·	·	·	·	·	·	X	·	·	·	8
	350	84	145	·	X	·	·	·	·	·	·	·	·	
4.2	85	60	−20	·	·	·	·	+	+	X	·	X	+	8
	186	73	−149	·	·	·	·	·	·	·	·	·	·	
4.4	319	61	18	·	·	·	·	X	X	+	X	X	X	8
	220	75	150	+	+	+	+	·	·	·	·	·	·	
5.0	323	63	28	·	·	·	·	+	X	+	·	+	X	8
	220	65	150	X	X	X	X	·	·	·	X	·	·	
4.4	35	45	54	·	·	·	·	·	·	·	·	·	·	6
	260	55	120	·	·	·	·	·	·	·	·	·	·	
4.5	292	70	10	·	·	·	·	X	X	X	X	X	X	6
	200	80	160	+	+	+	·	·	·	·	·	·	·	
4.5	259	40	9	·	·	·	·	X	X	X	X	X	X	7
	162	84	130	+	+	+	·	·	·	·	·	·	·	

†References: (1) *Choy and Boatwright* [1988]; (2) *Hasegawa and Wetmiller* [1980]; (3) *Hasegawa* [1977]; (4) *Herrman* [1973]; (5) *Herrmann* [1978]; (6) *Herrmann* [1979]; (7) *Herrmann* [1986]; (8) *Herrmann and Canas* [1978]; (9) *Herrmann et al.* [1982]; (10) *Nguyen and Herrmann* [1992]; (11) *Horner et al.* [1979]; (12) *Nabelek and Suarez* [1989]; (13) *North et al.* [1989]; (14) *Rogers et al.* [1980]; (15) *Schwartz and Christensen* [1988]; (16) *Taylor et al.* [1989]; (17) *Wetmiller et al.* [1984]; (18) *Yang and Aggarwal* [1981].

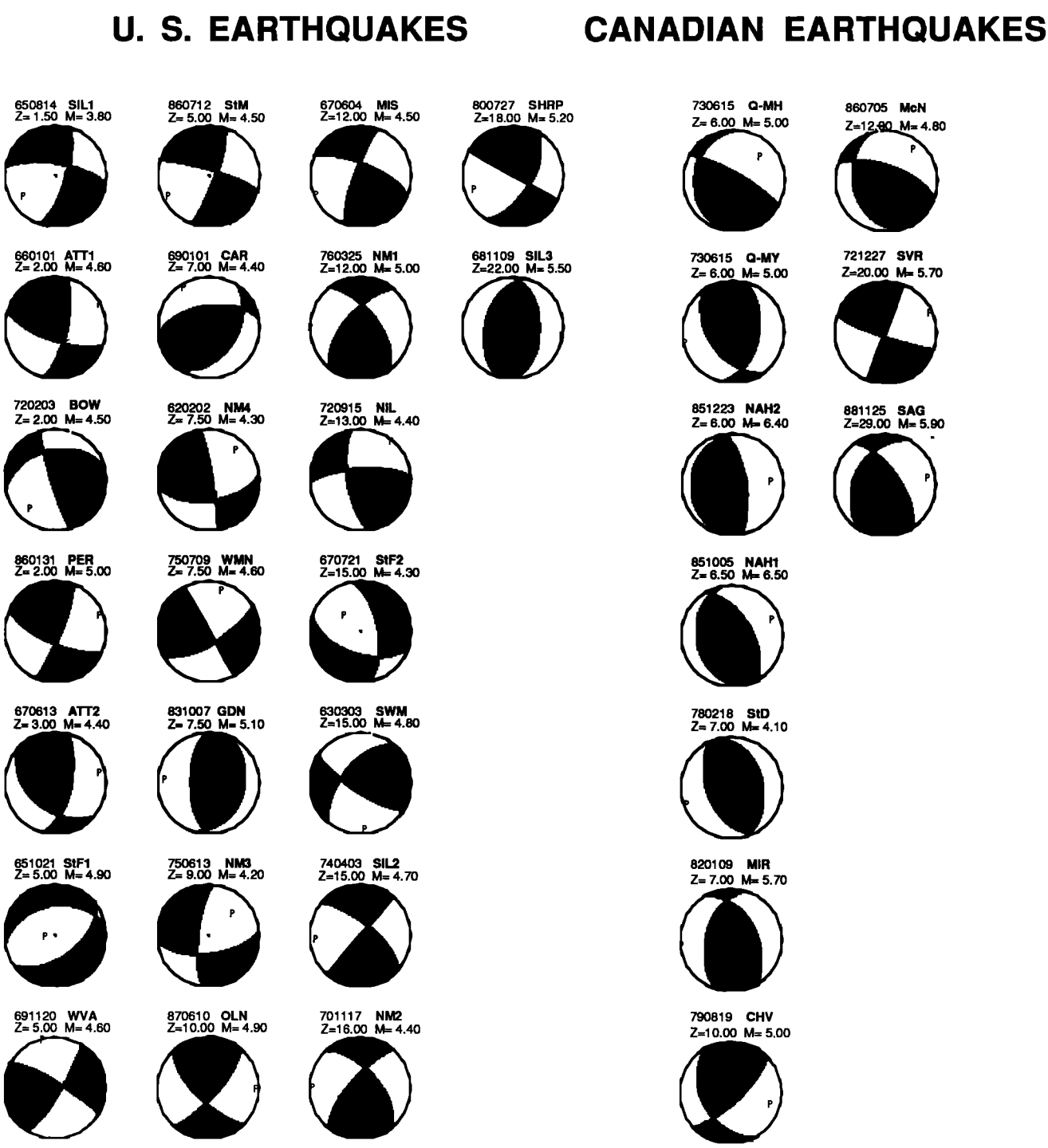

Fig. 2. Focal mechanisms for intraplate earthquakes considered in this study; mechanisms are separated into U.S. and Canadian subsets and are arranged by depth within each subset. Events are identified with codes from Table 1. Number on top left is depth in kilometers; number on top right is m_b.

in midplate North American are relatively rare and generally limited to the upper 2 km. The available data (primarily in the northeastern United States) generally indicate high horizontal compressive stresses (thrust regime) at shallow depths (less than about 0.5 km); in several cases a transition to a strike-slip faulting regime at greater depth has been documented with a uniform ENE $S_{H\max}$ orientation observed from the surface to depth [*Haimson and Doe*, 1983; *Nicholson et al.*, 1988; *Evans*, 1989].

In the absence of stress measurements at hypocentral depths, an alternate approach to constrain the magnitudes of in situ stresses is to assume that maximum stress differences in the crust are limited by the frictional strength of "optimally oriented" faults. This frictional faulting equilibrium model of stresses in the upper crust was first suggested by *Sibson* [1974] and is consistent with the notion that upper crustal stress magnitudes are in general limited by the stresses needed to cause slip on optimally oriented preexisting faults in a bulk fractured crust.

In terms of principal stresses, this limiting frictional

strength relationship (for a cohesionless Coulumb material) is given by [*Jaeger and Cook*, 1979, p. 89]

$$(S_1 - P_0)/(S_3 - P_0) =](\mu_c^2 + 1)^{1/2} + \mu_c]^2 \quad (5)$$

where μ_c is the coefficient of frictional sliding corresponding to the optimally oriented faults and P_0 is pore pressure. This equation is used to define the linear brittle portion of lithospheric strength profiles. These optimally oriented faults lie in the plane of S_2 and their orientation with respect to S_1 depends on the μ_c value selected [*Jaeger and Cook*, 1979, p. 89]:

$$\theta = 1/2[\pi/2 + \tan^{-1}\mu_c] \quad (6)$$

where θ is the angle between the fault normal and S_1. Literally thousands of laboratory experiments of frictional sliding on rocks have yielded rather uniform coefficients of friction, between 0.6 and about 1.0, largely independent of rock type (except for some very weak clays) [*Byerlee*, 1978]. Shallow stress measurements (to 3 km depth) from a variety of active tectonic settings have demonstrated that measured stress differences (S_1-S_3) do tend to lie along values theoretically predicted by (5) for frictional coefficients between 0.6 and 1.0 [*Pine et al.*, 1983; *Zoback and Healy*, 1984, 1992; *Stock et al.*, 1985; *Stock and Healy*, 1988; *Barton et al.*, 1988; *Baumgartner and Zoback*, 1989]. The attitudes of the optimally oriented faults can be determined by (6); for μ_c = 0.60, θ = 60.5° and for μ_c = 1.00, θ = 67.5. Thus the observed range in laboratory frictional coefficients predicts that the optimally oriented thrust faults should strike parallel to S_2 and dip between 29.5° and 22.5°, whereas the optimally oriented strike-slip faults should be vertical and strike between 29.5° and 22.5° from S_1.

In the analysis presented below, it is assumed that the magnitude of S_v is known and equal to the weight of the overburden. For simplicity, S_v is set equal to 1; thus all stress magnitudes are normalized by S_v. The ϕ values calculated from the geometric analysis of slip (equation (2)) can be substituted in equation (1) to provide constraints on the ratio of the principal stresses. A third constraint on stress magnitudes comes from the ratio, S_1/S_3 determined from the limiting strength of bulk fractured crust given in equation (5). Thus the magnitudes of all three principal stresses (normalized by S_v = 1) can be estimated.

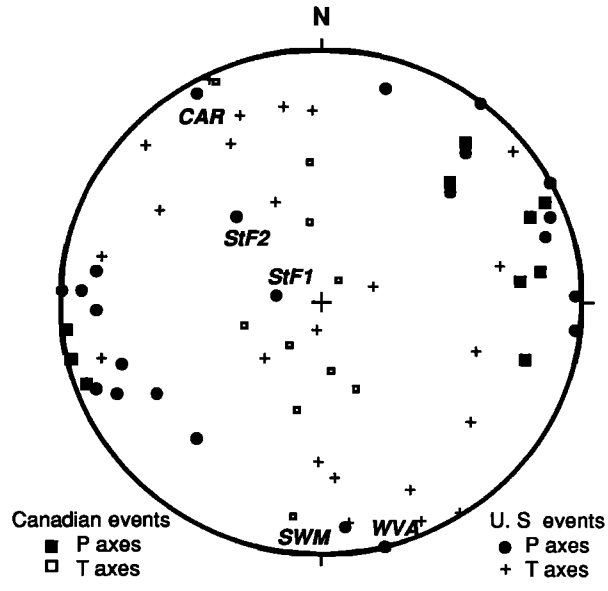

Fig. 3. Lower hemisphere stereoplot of P and T axes from all intraplate earthquakes considered in this study; Canadian and U.S. events are distinguished.

TABLE 2. Azimuth and Plunge of Stress Orientations for the Range of Uncertainty Considered, With Azimuths Referred to the Inferred $S_{H\max}$ Directions

	Horizontal Case	Case 1	Case 2
	Strike-Slip Faulting Regime		
S_1	$S_{H\max}$ ±10°/0°	$S_{H\max}$ ±0°/10°	$S_{H\max}$ ±0°/0°
S_2	$S_{H\max}$ ±10°/90°	$S_{H\max}$ +180°/80°	$S_{H\max}$ +90°/80°
S_3	$S_{H\max}$ (±10°) −90°/0°	$S_{H\max}$ −90°/0°	$S_{H\max}$ −90°/10°
	Thrust Faulting Regime		
S_1	$S_{H\max}$ ±10°/0°	$S_{H\max}$ ±0°/10°	$S_{H\max}$ ±0°/0°
S_2	$S_{H\max}$ (±10°) +90°/0°	$S_{H\max}$ −90°/0°	$S_{H\max}$ −90°/10°
S_3	$S_{H\max}$ ±10°/90°	$S_{H\max}$ +180°/80°	$S_{H\max}$ +90°/80°

The normal stress S_n acting on each fault plane and the shear stress τ acting in the direction of slip are then determined through tensor transformation. These stress values can, in turn, be substituted into (4) to determine the conditions for slip in these earthquakes. Fault zone pore pressure is computed assuming hydrostatic pore pressure (P_0 = $1.0/2.67S_v$ = $0.3737S_v$) regionally and that the friction on all faults is the same and equal to the critical value, μ_c. Because pore pressure is a physically measurable quantity in situ with real limits in the crust, i.e., pore pressure cannot exceed the least principal stress (S_3) magnitude or natural hydraulic fracturing will occur [e.g., *Lachenbruch*, 1980], the computed fault zone pore pressures are used to determine if the observed slip is frictionally likely (recall the phi calculation only determined if the observed slip is geometrically possible). In thrust faulting environments this pore pressure limit corresponds to the vertical stress, i.e., lithostatic pore pressure. In strike-slip and normal faulting environments the limit is lower and corresponds to the magnitude of the minimum horizontal stress, $S_{h\min}$. A second end-member possibility to explain slip is also considered; in this case, hydrostatic pore pressure is assumed both regionally and locally, and the ratio of shear to effective normal stress (the "apparent friction value") is calculated for each fault plane, allowing determination of a relative frictional coefficient (ratio of shear to effective normal stress) μ_f/μ_c for each slip plane. In this scenario, since the most optimally oriented faults are presumed to control the stress field, the only way that the less than optimally oriented faults can slip is that their apparent coefficient of friction must be less than the assumed regional frictional coefficient, μ_c.

RESULTS

All earthquakes were evaluated assuming both a thrust ($S_{H\max} > S_{h\min} > S_v$) and a strike-slip ($S_{H\max} > S_v > S_{h\min}$) faulting stress regime. This was done to determine if the contrast between thrust faulting mechanisms in southeastern Canada and the predominantly strike-slip mechanisms in central eastern U.S. indicated a real difference in stress regime between the two regions or if the contrast in mechanisms was simply a function of the attitude of fault

planes being selectively reactivated in a similar stress field [e.g., *Harmsen and Rogers*, 1986; *Zoback*, 1989].

Geometric Constraints

The initial result of the ϕ calculation was to determine which of the two nodal planes was a geometrically possible fault plane for a given stress orientation and stress regime. The results are shown in Figures 4*b* and 5*b* and the assessment of slip on all nodal planes is indicated on Table 1. A small center dot on Table 1 indicates that slip on the particular nodal plane was not geometrically compatible with the specific stress configuration. A plus indicates that the slip was geometrically possible but frictionally unlikely (by the criteria established here), and a cross indicates stress configurations for which slip was both geometrically possible and frictionally likely as described below. Note that a distinction is also made on all data plots (Figures 4–7) between the values computed for geometrically possible fault planes (open symbols) and the frictionally likely fault planes (solid symbols) based on the criterion that the computed fault zone pore pressure was less than the magnitude of the least principal stress ($P_f/S_3 < 1.0$, Figures 4*a* and 5*a*) as described below. On Figures 4–7 and in Table 1 the events are arranged by latitude from north to south. Note that Table 1 includes all 32 earthquakes considered for this study, whereas Figures 4–7 only list the 27 earthquakes which had a sense of slip compatible with the regional stress field. Both Table 1 and Figures 4–7 contain separate listings and results for the two focal mechanisms for the Quebec-Maine event of June 15, 1973, Q-MH and Q-MY.

Of the 32 earthquake focal mechanisms considered, five events had slip vectors incompatible with the regional stress field. These "incompatible" events include (1) the two nearly pure normal faulting events in southern Missouri (StF1 and StF2, Table 1): normal slip in these events is clearly incompatible with the regional compressive (S_1 horizontal) stress field and (2) the three central U.S. events in which the P axes are rotated nearly 90° with respect with the regional trend (SWM, CAR, WVA; see Figure 3): the resolved regional shear stress on these fault planes produced the wrong sense of slip (e.g., left-lateral instead of right-lateral). These five events require a local rotation or perturbation of the regional stress field or may simply be rather poorly constrained mechanisms (all events occurred prior to 1970 when station coverage was sparse and prior to much detailed local velocity structure information).

In the remaining 27 earthquakes the sense of slip was geometrically compatible with the inferred regional stress field in at least one of the two stress regimes considered. For 11 of the 27 events investigated, the requirement that the geometrically calculated ϕ value must lie between 0 and 1 uniquely selected one of the two planes as the "true fault plane" for the full five stress configurations for one of the two stress regimes considered (i.e., one nodal plane is marked with either a cross or a plus in all five stress configurations in one of the two stress regimes and the other plane is marked with five dots). In another nine of the 27 events, a single nodal plane was selected for four out of five of the stress configurations (in all cases the excluded configuration was one of the tilted axes cases). For two events (ATT1 and NIL), the selected "true fault plane" switched between nodal planes within the range of stress orientations considered; however, for any given stress tensor orientation, only one of the two nodal planes had an allowable ϕ value. This unique selection of one nodal plane as a fault plane for a given stress tensor orientation has been reported previously for other focal mechanism data sets [e.g., *Bjarnason and Pechmann*, 1989; *Carey-Gailhardis and Mercier*, 1987] and, as mentioned above, has also been demonstrated theoretically [*Gephart*, 1985].

Focal mechanisms for two events, NM3 and NM4 (at 36.5°N), had geometrically possible slip vectors over only a very limited range of the stress orientations considered. As indicated in Table 1, in all but one case the selected fault plane for these events was striking in or within <10° of the inferred regional $S_{H\max}$ direction (N85°E). Slip was geometrically possible in these events because the fault plane was dipping and the slip vector was oblique. Although three of the possible stress/fault configurations for these two events were found to be frictionally likely (see below), it is also likely that the inferred N85°E regional $S_{H\max}$ orientation is not valid in the region of these earthquakes. Both NM3 and NM4 occurred within the New Madrid seismic zone, the most seismically active intraplate region in central and eastern North America [e.g., *Mitchell et al.*, 1991]. Both events are located at the northern end of the main seismic zone, near a cross trend of seismicity associated with an inferred left-stepping offset in the main zone. Block rotation or complex fault interaction may be a source of a localized stress anomaly in this region. Slip in both events would be frictionally consistent with a strike-slip regime with a more northerly $S_{H\max}$ orientation (e.g., N60°E), requiring a counterclockwise rotation of the horizontal stress axes in this region. Alternately, mechanisms for these two events may not be reliable, as they were determined prior to detailed knowledge of velocity structure in the New Madrid region, particularly the low velocity of the rift zone sediments [e.g., *Andrews et al.*, 1985].

Physically, the ϕ values shown in Figures 4*b* and 5*b* indicate the magnitude of the intermediate stress, S_2, relative to the maximum, S_1, and minimum, S_3, stress values (equation (1)), and hence a separate ϕ value was calculated for each fault in each stress regime. In a thrust faulting regime, the $\phi = 0$ end-member ($S_2 = S_3$) corresponds to the case when $S_{h\min} = S_v$ or transitional to strike-slip faulting, whereas the $\phi = 1$ end-member ($S_1 = S_2$) corresponds to $S_{h\max} = S_{h\min}$ or radially isotropic compression. In a strike-slip faulting stress regime the $\phi = 0$ end-member ($S_2 = S_3$) corresponds to a stress state transitional to a thrust faulting

Fig. 4. (Opposite) Results of frictional faulting analysis for a thrust faulting stress regime, computed values are given for the each of the five possible stress tensor configurations for each geometrically possible fault plane for each event. Reference lines on each plot are discussed in text. (*a*) Normalized fault zone pore pressure values (relative to the minimum principal stress, the lithostat, P_f/S_v) which were used to determine which fault plane/stress configurations are frictionally likely, i.e., those fault planes whose slip can occur with a normalized pore pressure less than 1.0 ($P_f/S_v < 1.0$). On this and all subsequent data plots these frictionally likely fault plane/stress configurations are shown with solid symbols; values for geometrically possible but frictionally unlikely ($P_f/S_v \geq 1.0$) fault plane/stress configurations are shown with open symbols. (*b*) Computed ϕ values. (*c*) Angle between fault strike and $S_{H\max}$ azimuth; note that there is a 20° range in these angles for the horizontal case corresponding to the ±10° uncertainty range in $S_{H\max}$ azimuths considered. (*d*) Fault dips.

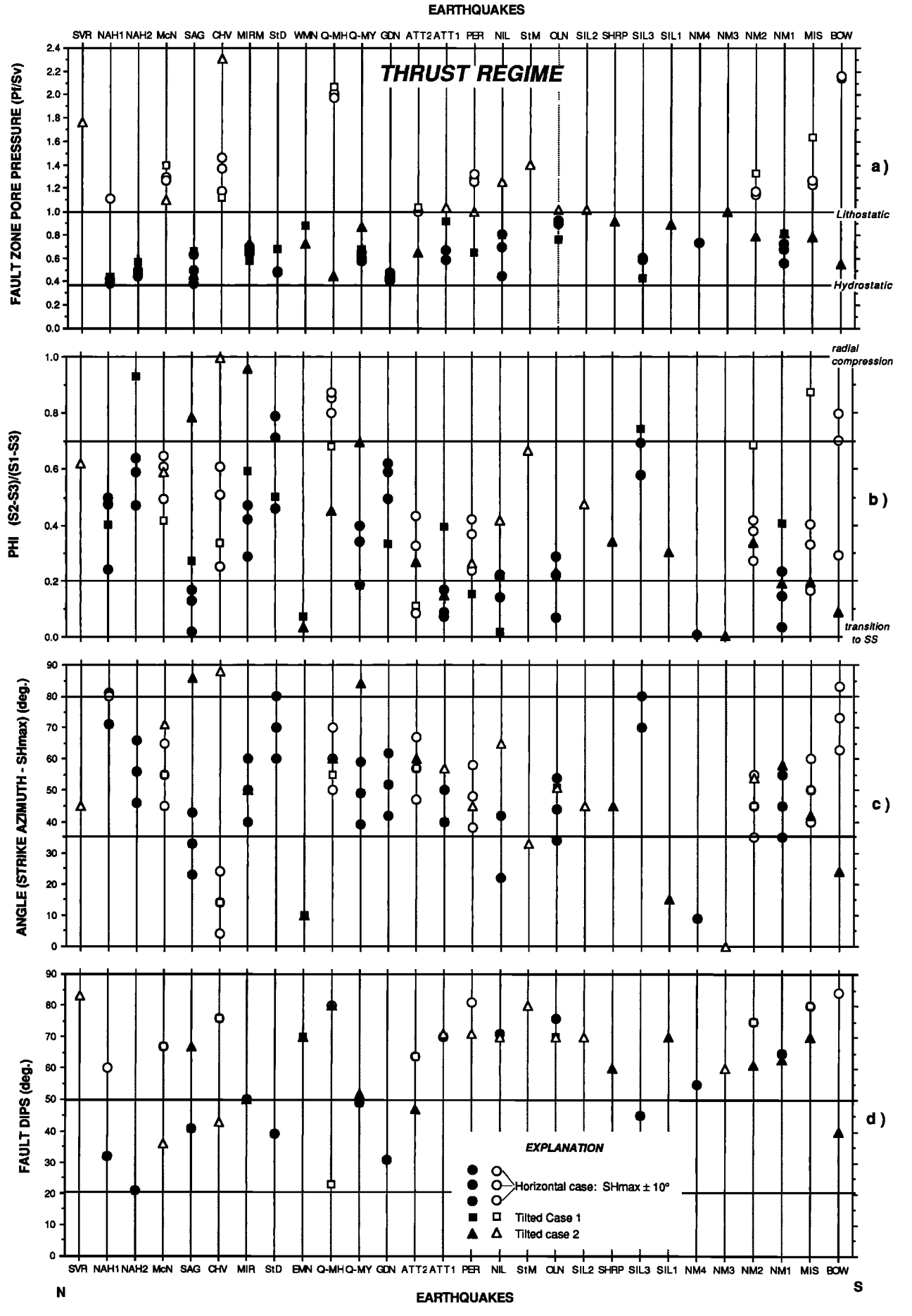
EARTHQUAKES
SVR NAH1 NAH2 McN SAG CHV MIRM StD WMN Q-MH Q-MY GDN ATT2 ATT1 PER NIL StM OLN SIL2 SHRP SIL3 SIL1 NM4 NM3 NM2 NM1 MIS BOW
THRUST REGIME
FAULT ZONE PORE PRESSURE (Pf/Sv)
a)
Lithostatic
Hydrostatic
PHI (S2-S3)/(S1-S3)
radial compression
b)
transition to SS
ANGLE (STRIKE AZIMUTH - SHmax) (deg.)
c)
FAULT DIPS (deg.)
d)
EXPLANATION
Horizontal case: SHmax ± 10°
Tilted Case 1
Tilted case 2
SVR NAH1 NAH2 McN SAG CHV MIR StD EMN Q-MH Q-MY GDN ATT2 ATT1 PER NIL StM OLN SIL2 SHRP SIL3 SIL1 NM4 NM3 NM2 NM1 MIS BOW
N
EARTHQUAKES
S

regime and a $\phi = 1$ end-member ($S_1 = S_2$) corresponds to a transition to normal faulting stress regime. The corresponding attitudes of the selected fault planes are indicated in terms of the angle between fault strike and $S_{H\max}$ direction (Figures 4*c* and 5*c*) and dip (Figures 4*d* and 5*d*).

The N-S variation in stress regime across southeastern Canada/northeastern United States is obvious in a comparison of the events with frictional likely ϕ values (solid symbols) in Figures 4*b* and 5*b*. Inspection of the ϕ values for the thrust faulting regime (Figure 4*b*) indicates that all of the 27 events had a slip plane geometrically compatible with this thrust regime for at least one of the assumed stress tensor orientations. However, many of the events, particularly the more southerly events (StM and south), had permissible slip vectors in a thrust regime over a very limited part of the range of stress configurations considered, and in many cases this slip was frictionally unlikely. In detail, in Figure 4*b* there appears to actually be a systematic north to south decrease in range of ϕ values for the frictionally likely events across southeastern Canada (from MIR to ATT1); this north to south decrease may be indicating a real lateral variation in relative stress magnitudes responsible for the contrast in faulting styles between southeastern Canada and the central eastern United States. Most of the frictionally likely slip planes in the thrust regime for the northern events (north of ATT1) had intermediate ϕ values, in the range of 0.2–0.7; although the SAG event and the more southerly U.S. events WMN, OLN, and NM1 with thrust compatible slip all had very low ϕ values, close to the strike-slip end-member. Very high ϕ values (>0.9, a stress state approaching compression) was frictionally possible only for two events, both in a tilted stress axes case.

As shown in Figure 5*b*, nearly all events south of GDN were both frictionally and geometrically compatible with a strike-slip faulting regime with ϕ values <0.55, closer to the thrust faulting end-member. Furthermore, for most of the events from GDN north, geometrically compatible slip was possible in a strike-slip regime over only a limited part of the range of stress configurations considered, and in many cases this slip coincided with very high ϕ values, close to the normal faulting end-member. In fact, north of ATT2 (42.9°) none of the earthquakes were found to have slip frictionally compatible with a strike slip regime except the previously mentioned Arctic island strike-slip event (SVR) and part of the range considered for the western Minnesota event, WMN. As shown in Figure 5*c*, all the northerly geometrically compatible fault planes high ϕ values in the strike-slip regime strike at very high angles to $S_{H\max}$ (angle between strike and $S_{H\max}$ azimuth between 80° and 88°). Thus, while the direction of slip on these planes which are oriented nearly perpendicular to $S_{H\max}$ was geometrically possible with the high ϕ values, it is not surprising that this reverse oblique slip was not frictionally likely in a strike-slip stress regime transitional to a normal faulting stress regime.

Frictional Constraints

For 25 of the 27 events with geometrically possible slip vectors, this slip was determined to be also frictionally likely in at least one of the two stress regimes as shown in Table 1 with the crosses and on Figures 4*a* and 5*a*. Several of the events had frictionally possible slip vectors in both regimes; however, no single stress regime could explain slip in all the events. As described in detail above, the frictionally likely events for the two regimes shown by the solid symbols in Figures 4*a* and 5*a* clearly demonstrate the N to S variation in stress regime across southeastern Canada/northeastern United States and number of events within a "transition region" between about 43° and 41.5°N (from ATT2 south to NIL) had frictionally likely slip compatible with both regimes over a limited range of orientations considered.

As shown in Figures 4*a* and 5*a*, the required local fault zone pore pressures for the "frictionally likely" events in both stress regimes were generally moderate, in the range of 0.4–0.8, not superlithostatic [e.g., *Sibson*, 1989*a*, 1990]. In the thrust faulting regime these pore pressures represent true values relative to the lithostat (recall that hydrostatic pore pressure is 0.37 of lithostatic). In the strike-slip stress regime, however, the effective pore pressure limit was the magnitude of the least principal stress, $S_{h\min}$. The actual pore pressure values (relative to the lithostat) in the strike-slip faulting regime are given in Figure 6. Slip in the frictionally likely fault planes in the strike-slip regime requires actual pore pressures in the range of 0.4–0.75 of the lithostat.

Three focal mechanisms (McN, CHV, and Q-MH) had slip that was geometrically possible but either strictly frictionally unlikely ($P_f/S_3 > 1$) or probably unlikely ($P_f/S_3 > 0.95$) in any stress orientation in either of the two regimes. All three of these focal mechanisms were unusual in that the nodal planes with steeper rakes which were geometrically compatible with a thrust regime were rather steeply dipping (62°–80°), whereas the orthogonal nodal plane with more shallow rakes which were geometrically compatible with a strike-slip stress regime had rather shallow dips (23°–34°). Both configurations resulted in a high normal stress across the fault plane; hence these fault/slip configurations were frictionally unlikely and required extremely high pore pressures, far exceeding the lithostat (Figures 4*a* and 5*a*). Note that the alternate mechanism available for the Q-M event, Q-MY, was frictionally compatible with a thrust faulting regime over the full uncertainty range of stress orientations considered.

An alternate end-member used to evaluate the likelihood of slip is one in which pore pressure, both regionally and locally, is assumed constant and equal to hydrostatic and slip is a result of a lowered frictional coefficient within the fault zone; in this case the local relative frictional coefficients required for slip, μ_f/μ_c (relative to μ_c the assumed friction on optimally oriented faults controlling regional stress mag-

Fig. 5. (Opposite) Results of frictional faulting analysis for strike-slip faulting stress regime, computed values are given for the each of the five possible stress tensor configurations for each geometrically possible fault plane for each event. Reference lines on each plot are discussed in text. (*a*) Normalized fault zone pore pressure values (relative to the minimum principal stress, $S_3 = S_{h\min}$, P_f/S_3) which were used to determine which fault plane/stress configurations are frictionally likely, i.e., those fault planes whose slip can occur with a normalized pore pressure less than 1.0 ($P_f/S_3 < 1.0$). On this and all subsequent data plots these frictionally likely fault plane/stress configurations are shown with solid symbols; values for geometrically possible but frictionally unlikely ($P_f/S_3 \geq 1.0$) fault plane/stress configurations are shown with open symbols. (*b*) Computed ϕ values. (*c*) Angle between fault strike and $S_{H\max}$ azimuth; note that there is a 20° range in these angles for the horizontal case corresponding to the ±10° uncertainty range in $S_{H\max}$ azimuths considered. (*d*) Fault dips.

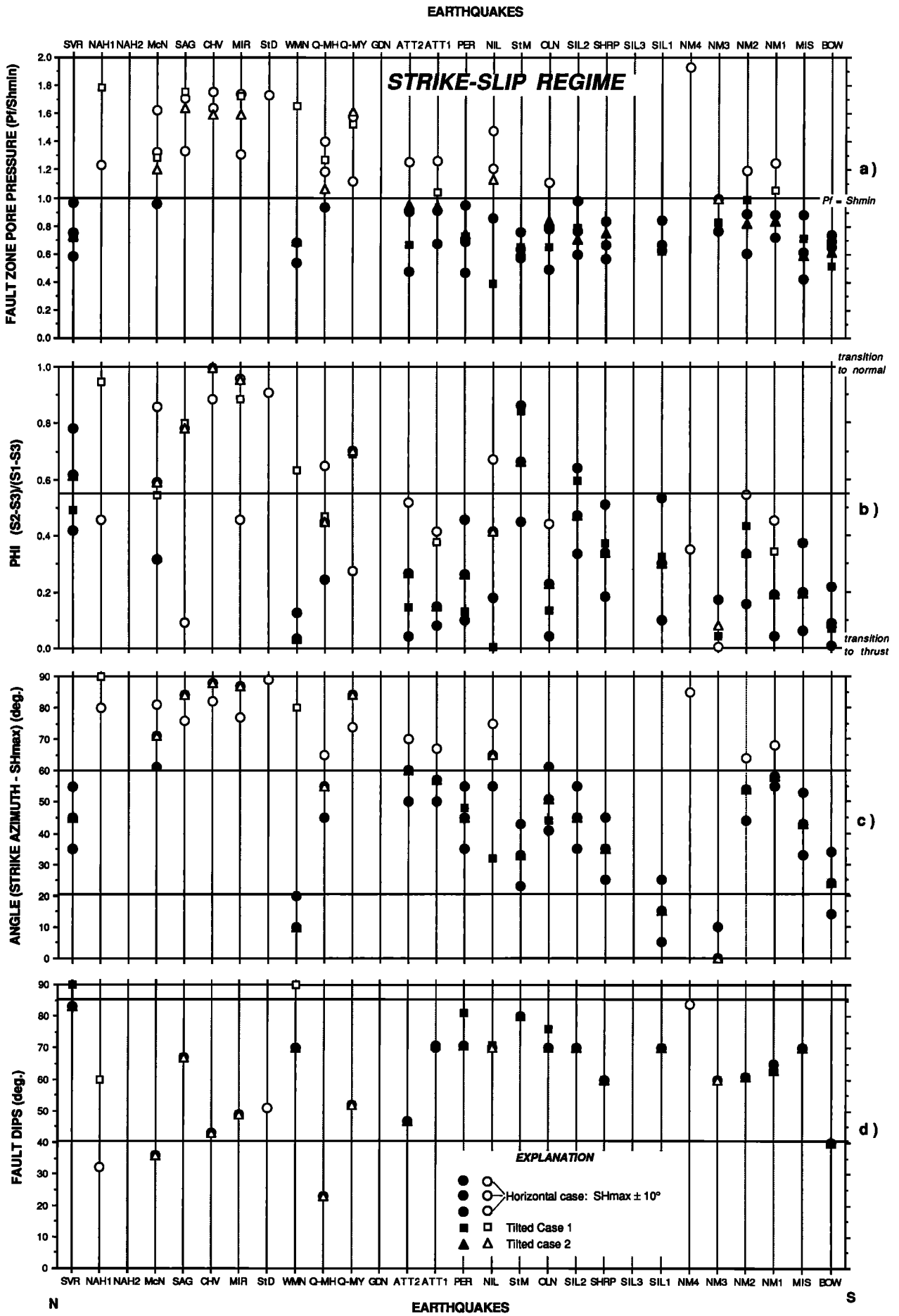
EARTHQUAKES
SVR NAH1 NAH2 McN SAG CHV MIR StD WMN Q-MH Q-MY GDN ATT2 ATT1 PER NIL StM CLN SIL2 SHRP SIL3 SIL1 NM4 NM3 NM2 NM1 MIS BOW
STRIKE-SLIP REGIME
FAULT ZONE PORE PRESSURE (Pf/Shmin)
a)
Pf = Shmin
PHI (S2-S3)/(S1-S3)
b)
transition to normal
transition to thrust
ANGLE (STRIKE AZIMUTH - SHmax) (deg.)
c)
FAULT DIPS (deg.)
d)
EXPLANATION
Horizontal case: SHmax ± 10°
Tilted Case 1
Tilted case 2
N
S
EARTHQUAKES

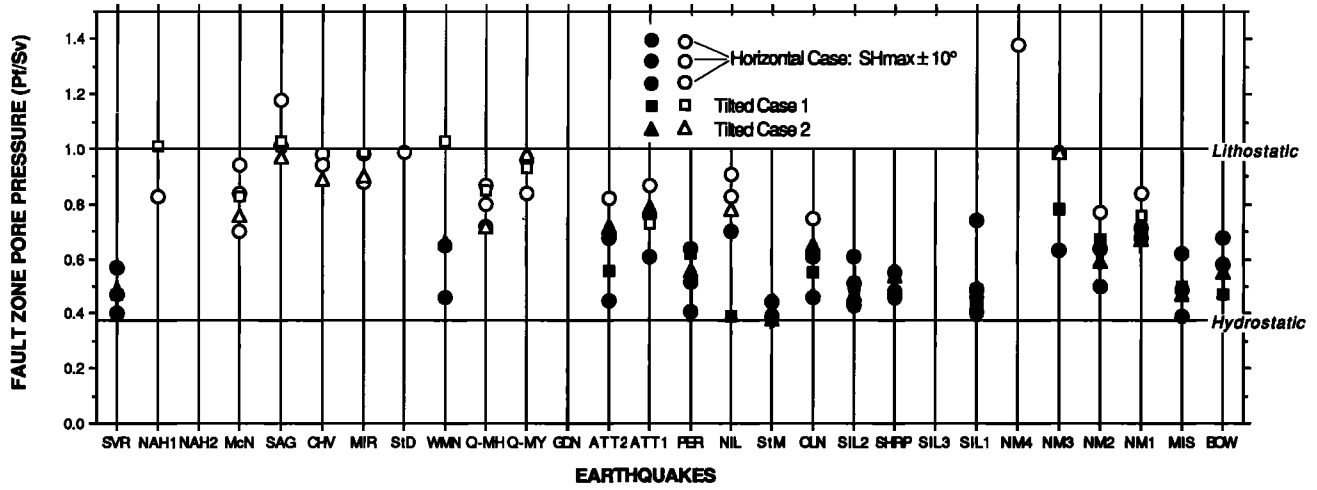

Fig. 6. Fault zone pore pressure values normalized to the lithostat (P_f/S_v) for the strike-slip faulting stress regime, these values correspond to the fault zone pore pressures shown in Figure 5*a* which were normalized by the minimum principal stress, $S_3 = S_{h\min}$. As in Figures 4 and 5, solid symbols indicate fault/stress configurations considered frictionally likely; open symbols are geometrically possible but frictional unlikely fault/stress configurations.

nitudes) were calculated from (4) using stress magnitudes determined from (5) and are shown in Figures 7*a* and 7*b*. Since the faults used in this analysis all exhibited oblique slip and were presumed to be less than optimally oriented, the local frictional coefficients μ_f must be less than μ_c, $\mu_f/\mu_c < 1.0$.

As shown in Figure 7*a*, the relative frictional coefficients (μ_f/μ_c) in the thrust faulting regime generally ranged from 0.4 to 0.95. Most of the fault planes determined to be frictional likely from the pore pressure constraint discussed above (and indicated by the solid symbols on Figures 4–7) had relative coefficients in the range of $0.6–0.95\mu_c$. These relative coefficients can be converted to actual coefficients by multiplying by a value for μ_c. As mentioned previously, laboratory-determined frictional coefficients for nearly all rocks in upper crustal conditions range between 0.6 and 1.0, although some clays were found to have coefficients as low as 0.4 [*Byerlee*, 1978]. Using a representative value of $\mu_c = 0.65$, the "actual" frictional coefficients required for the faults slipping in the thrust faulting regime vary between 0.26 and 0.62, with the pore pressure determined "frictionally likely" planes having "actual" coefficients between 0.39 and 62, a range compatible with the laboratory observations.

Relative frictional coefficients computed for the strike-slip case were widely scattered from ~0.0 to 0.95 (Figure 7*b*). However, the relative friction coefficients for the fault planes determined to be frictional likely from the pore pressure constraint discussed above (and indicated by the solid symbols on Figures 4–7) were nearly all >0.5, with most in the range of 0.6–0.95. These relative coefficients corresponding to "actual" frictional coefficients between 0.39 and 0.62 using $\mu_c = 0.65$, the same range found for the thrust regime. The northern events requiring extremely low normalized frictional coefficients (NAH1 to StD) were found to be frictionally unlikely in a strike-slip regime by the pore pressure criterion as indicated by the open symbols.

Note that pore pressure determined frictionally likely slip was possible at lower relative frictional coefficients (<0.5) for several stress orientations for events WMN, SIL1, and NM4 in the thrust regime and for events SIL1 and NM3 in the strike-slip regime. As shown in Figures 4*c* and 5*c*, the angle between the fault strike and the $S_{H\max}$ azimuth is quite small (<15°) for all of the frictionally likely stress/slip configurations for these events; this small angle results in a relatively small component of normal stress across the fault plane (provided that the two horizontal stresses are not equal). The low values of relative frictional coefficients computed for these planes simply indicate a low value for the ratio of shear to normal stress on these fault planes. Thus the slip was found to be frictionally likely using the pore pressure criterion only because the somewhat elevated pore pressure reduced the already low normal stress across these faults but has no effect on the shear stress.

Inspection of Figures 4*c*, 4*d*, 5*c*, and 5*d* permits some characterization of the attitudes of fault planes frictionally compatible with a thrust faulting regime (primarily the events from GDN north) and a strike-slip faulting regime (SVR and WMN and events south of GDN). Recall from equation (6) that the optimally oriented faults strike in the plane of S_2 and the angle between S_1 and the fault is determined by μ_c. For $\mu_c = 0.65$ this angle is 28.5°. Thus, in a thrust faulting stress regime with true horizontal and vertical principal stresses, the optimal fault strikes in the $S_{h\min}$ direction (perpendicular to $S_{H\max}$), dips 28.5°, and has pure dip-slip motion. As shown in Figures 4*c* and 4*d*, the strikes of the frictionally likely fault planes in a thrust regime in this study varied between about 35° and 80° of the $S_{H\max}$ orientation, and the corresponding dips were in the range of 20°–50°. In a strike-slip stress regime with horizontal and vertical stresses the optimally oriented faults are vertical and strike 28.5° from the $S_{H\max}$ direction. As shown in Figures 5*c* and 5*d*, the fault planes frictionally compatible with a strike-slip stress regime generally had strikes between 20° and 60° of the $S_{H\max}$ direction and dips between 40° and 80°, with most dips in the 60°–75° range.

The wide range in angles between fault strike and $S_{H\max}$ azimuth in the thrust regime and the range of dips in the strike-slip regime demonstrates the influence of fault attitude (relative to stress orientation) combined with relative stress magnitudes (ϕ value) which produces the observed oblique

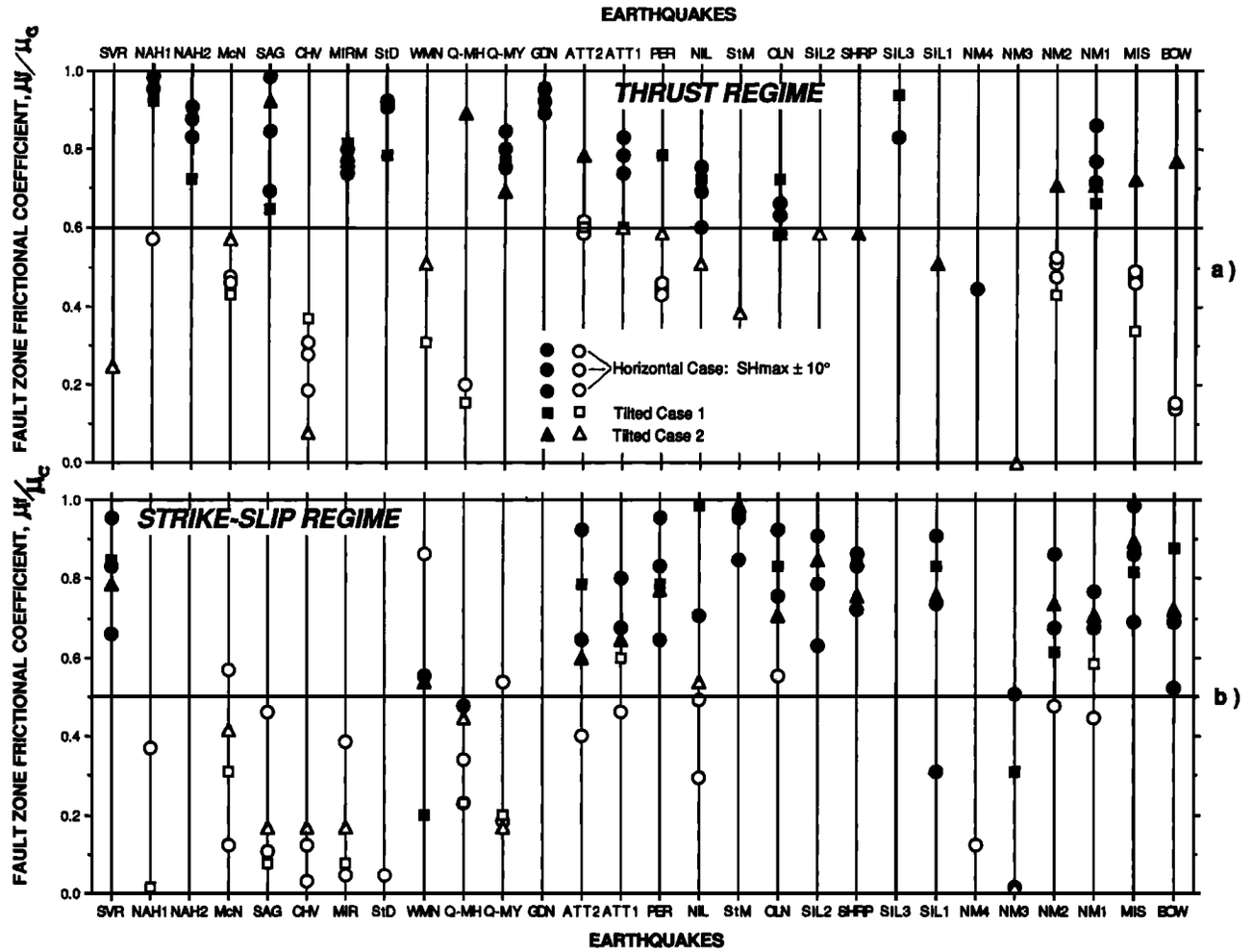

Fig. 7. Normalized fault zone frictional coefficients (μ_f/μ_c). (*a*) Thrust faulting stress regime. (*b*) Strike-slip faulting stress regime. As in Figures 4 and 5, solid symbols indicate fault/stress configurations considered frictionally likely; open symbols are geometrically possible but frictional unlikely fault/stress configurations (based on the pore pressure constraint shown in Figures 4*a* and 5*a*).

slip in these events. Because of this geometric complexity, some of the frictionally likely fault planes are far from optimal orientations. For instance, in some cases, slip was possible on rather steep faults in a thrust regime with only modest increase in pore pressure; e.g., slip in the Miramichi, New Brunswick, event of January 9, 1982 (MIR), was possible over the full range of stress orientations considered on a fault plane which dips 50° and yet the required pore pressures were only between 0.58 and 0.71 of lithostatic (Figure 4*a*). This result is in marked contrast to superlithostatic pore pressures inferred from a frictional faulting analysis of slip in this event ignoring the oblique component of slip [*Sibson*, 1989a]. Similarly, oblique slip was frictionally possible on rather shallowly dipping faults in a strike-slip regime with only modest increase in pore pressure. For example, slip in the Bowman, South Carolina, event of February 3, 1972 (BOW), was possible over the entire range of stress orientations considered on a fault plane dipping 40° with pore pressures only between 0.47° and 0.57 of lithostatic (Figure 6).

Note that in some cases, frictionally likely slip compatible with a thrust regime occurred on very steeply dipping fault planes (dips 60°–75°); in many cases this slip was limited to the tilted stress axes configurations in which the effective dip was shallower than the true dip. However, for several events (SAG and more southerly events WMN, ATT1, NIL, OLN, NM1), slip on moderate to steep planes (dips between 41° and 76°) was frictionally possible over much of the stress orientation range considered. As shown in Figure 4*b*, all of these events were all associated with very low ϕ values ($\phi <$ 0.2), indicating a stress regime near the strike-slip end-member.

DISCUSSION

Hypothesis Evaluation

Accepting that the focal mechanisms for the 32 intraplate earthquakes considered in this study are an accurate representation of the faulting that occurred in these events, the results of the stress analysis described above permit assignment of the events to one of the two hypotheses for intraplate seismicity discussed in the introduction.

Hypothesis 1 is the reactivation of well-oriented preexisting faults in a uniformally oriented regional stress field with principal planes oriented approximately horizontally and

vertically. The majority of the earthquakes, 23 of 32 events (72%), have slip vectors which are geometrically and frictionally compatible with the regional stress field. No single stress regime could geometrically (nor therefore frictionally) explain slip in all these events, there appears to be a general north to south variation in relative stress magnitudes from southeastern Canada to the central eastern United States. As a result, slip in the events north of about 41°–43° (the U.S.-Canada border region) requires a thrust faulting stress regime, whereas slip in the central eastern U.S. events is generally compatible only with a strike-slip stress regime. While the source of the orientation and general compressive nature of the regional stress field appears related to far-field plate-driving forces, this contrast in stress regimes requires a more local source of lateral variation of relative stress magnitudes.

Assuming a constant coefficient of friction on all faults, only moderate, not superlithostatic [e.g., *Sibson*, 1990], pore pressures are required for reactivation of these faults in both the thrust and strike-slip regimes varied between about 0.4 and 0.80 of lithostatic (where hydrostatic is 0.37 of lithostatic). Alternately, if hydrostatic pore pressure is assumed everywhere, then the frictional coefficients required for reactivation of these faults are generally greater than one half of μ_c, the assumed frictional coefficient on the optimally oriented faults controlling crustal strength. In reality, slip may result from a combination of both factors: slightly elevated pore pressure and a somewhat reduced coefficient of friction.

The fault planes frictionally compatible with a thrust faulting regime generally had strikes between 35° and 80° of the $S_{H\max}$ direction and dips between 20° and 50°. Those frictionally compatible with a strike-slip faulting regime had strike between 20° and 60° of the $S_{H\max}$ direction and dips between 40° and 80°, with most dips between 60° and 70°. The attitudes of these fault planes are consistent with suggestion of slip on preexisting faults rather than formation of new faults based on comparisons of laboratory studies on frictional sliding of preexisting faults with the measured shear strength of intact rock. For example, *Raleigh et al.* [1972] concluded that preexisting faults are probably reactivated (rather than having new faults develop) when the angle between the fault and the maximum stress in the plane of the slip vector is between about 25° and 55°. This angle generally corresponds to the dip of the thrust faulting planes (found in this study to be between 20° and 50°) and to the difference between the strike and $S_{H\max}$ azimuth in a strike-slip faulting case (found in this study to be between 20° and 60°).

Hypothesis 2 is the localized stress perturbation. Five of the 32 events studied clearly fell into this category, two other events are possibly in this category:

1. StF1 and StF2, two normal faulting earthquakes in the St. Francois Mountains with nearly orthogonal T axes, are clearly anomalous with respect to each other and with respect to the regional compressional stress regime. This suggests local complexity in the stress field within one of the few exposed regions of Precambrian basement in the east central United States.

2. SWM, CAR, and WVA are central United States strike-slip earthquakes that have slip vectors incompatible with the sense of shear inferred from the regional stress orientations. In all three cases these earthquakes have P axes nearly 90° different than those of nearby earthquakes (see Figure 1).

3. NM3 and NM4 have fault planes striking parallel (within 1°) to the inferred regional $S_{H\max}$ direction. A low ratio of shear to normal stress on these faults could permit slip with elevated pore pressures over part of the range of stress orientations considered. However, it is equally likely that the slip is the result of a local stress rotation related to fault interactions or block motion within this active seismic region.

Interestingly, all five events which are clearly incompatible with the regional stress field occurred prior to 1970 before regional seismic networks had begun to be established and there was little detailed knowledge of crustal velocity structure. The mechanisms for the two New Madrid events were also done before determination of detailed velocity structure within the New Madrid rift.

Unclassified events are the final events (McN, CHV) and an alternative focal mechanism for one event (Q-MH) that have slip vectors geometrically consistent with the regional stress field but were not found to have frictionally likely slip as they are very poorly oriented for reactivation in the inferred regional stress field. Slip in these events over nearly the entire range of stress orientations considered in either a thrust or strike-slip regime requires either extremely weak faults (frictional coefficients less than 0.30) or superlithostatic pore pressures. Alternately, the events may result from local stress rotations (anomalies) not detected with current stress data sampling and hence would fall into the hypothesis 2 category, or the focal mechanisms may be more poorly constrained than assumed (both McN and CHV are based only on first motions, no waveform modeling). The Q-MH event was constrained by surface wave modeling and first motions; however, a more recent solution, Q-MY (based only on first motions but with additional data than available when Q-MH was done) yielded quite reasonable results, compatible with the majority of the events in this category. Recall that *Wetmiller* [1975] had actually found a normal fault solution for this event; thus it is likely that the focal mechanism for this event is very poorly resolved.

Fault Plane Identification and Implications for the Nature of Seismic Zones

Identification of the actual fault plane for all the earthquakes considered in this study through the ϕ calculation is a powerful piece of information which permits further analysis of the in situ conditions accompanying faulting as well as the relationship of the fault planes to preexisting structures. Unfortunately, there are few independent checks on which of the two nodal planes is the actual fault plane for most of the intraplate events. In fact, the proper identification of which of the two nodal planes is the actual fault through this analysis could be considered a test of the assumption that the regional stress field is characterized by approximately horizontal and vertical planes.

Likely fault planes have been identified for eight of the earthquakes considered in this study; in seven of eight of these events this identification was based on aftershock distributions; in one case (MIR) it was based on an inversion of duration measurements made on broadband velocity pulse shapes [*Choy et al.*, 1983]. A good distribution and a large number of aftershocks clearly defined fault planes for the

two largest events, NAH1 and NAH2 [*Wetmiller et al.*, 1988]. As shown in Table 1, slip in both these events was found to be compatible with only one stress regime and a single fault plane was identified. In both cases the analysis presented here correctly identified the fault plane inferred independently by aftershock distribution. The analysis also uniquely selected the fault plane identified by *Choy et al.* [1983] for the MIR event and the NE trending plane identified for the SHRP, the strike and dip of which were moderately well-constrained by aftershocks. The analysis did not uniquely identify the fault planes inferred from aftershock distributions for the four remaining events SAG, GDN, PER, and OLN. In two cases the fault planes (OLN, northeast striking plane [*Langer and Bollinger*, 1991], and GDN, west dipping plane [*Dawers and Seeber*, 1991]) were moderately well constrained, and the analysis selected the opposite plane for all but one stress configuration. In the remaining two earthquakes, possible fault planes were inferred (SAG, east dipping plane [*North et al.*, 1989], and PER, north-northeast striking plane [*Nicholson et al.*, 1988]) from a small number and tight cluster of aftershocks, but both set of authors concluded that the evidence for the selection of the plane was not conclusive.

Determination of the dips of the selected fault planes for these events can provide a basis for evaluation of the observation that much of the intraplate seismicity in North America occurs in regions with an earlier history of rifting [*Johnston*, 1989; *Johnston and Kantor*, 1990; *Mitchell et al.*, 1991]. The 60°–75° dips determined for most of the frictionally likely fault planes currently being reactivated in an oblique strike-slip-reverse mode in the central and eastern United States (Figure 5*d*) are slightly greater than the 35°–60° range of dips of active normal faults interpreted from geodetic and focal mechanism data in both the Basin and Range province [*Smith et al.*, 1989] and around the world [*Jackson*, 1987]. The 20°–50° dips of the frictionally likely fault planes being reactivated in the thrust regime (Figure 4*d*) also overlap the dips of currently active normal fault planes but are somewhat shallower. However, results of seismicity and other geophysical studies in the New Madrid seismic zone, one of the most seismically active intraplate regions in North America, indicate the difficulty in ascribing intraplate seismicity to simple reactivation of old rift-related normal faults. These detailed studies have defined a major vertical strike-slip fault zone striking along the axis of a NE trending late Precambrian–early Paleozoic rift [*Hildebrand et al.*, 1977; *Hamilton and Zoback*, 1982; *Zoback et al.*, 1980; *Andrews et al.*, 1985]. While the old rift structure in general seems to have played a role in localizing seismicity, the main seismic zone occurs down the center of the approximately 70-km-wide rift; the primary basin-bounding fault zones along the rift margins (with geophysically determined offsets of 4–5 km) are currently largely aseismic [*Andrews et al.*, 1985].

Lateral Stress Gradient Due to Superposed Glacial Rebound Stresses?

The geometric and frictional analysis demonstrated that the contrast between dominantly thrust focal mechanisms in southeastern Canada and dominantly strike-slip focal mechanisms in the central eastern United States previously noted by *Hasegawa et al.* [1985] and *Talwani and Rajendran* [1991] cannot be explained as a result of the complexity of slip on obliquely oriented preexisting faults with minor variations of ϕ values in a single stress regime [e.g., *Angelier*, 1979; *Harmsen and Rogers*, 1986; *Zoback*, 1989]. The contrast in stress regime (which is demonstrated in the mechanisms between CHV to SIL3 on Table 1) requires a lateral variation in the relative magnitudes of the horizontal stresses. Since the $S_{H\max}$ orientation is uniform across these two regions (Figure 1), the principal stress axes are the same in both regions, and the change from a strike-slip regime in the central eastern United States to a thrust regime in southeastern Canada–U.S. border region requires a northward increase in horizontal stress magnitudes. *Talwani and Rajendran* [1991] noted that this change in focal mechanism style occurs close to the southern boundary of the old ice sheet and suggested that the lateral stress variation may be due to superimposed rebound-related flexural stresses in response to the removal of the Pleistocene ice sheet that extended south of the Great Lakes (the southern limit of rebound warping is shown on Figure 1). *Hasegawa and Basham* [1989] also noted the correlation of high levels of seismicity, steep gradients in free-air gravity, and steep gradient in postglacial uplift (post-8000 years B.P.) along the northeastern periphery of the Canadian shield and concluded that there may be a causal relationship.

A detailed regional study of shallow stress magnitudes measured in oil wells on the Appalachian Plateau by *Evans* [1989] also indicated a lateral variation in horizontal stress magnitudes in the northeastern United States. Evans found that measured $S_{h\min}/S_v$ ratios in the upper 2 km (below a regionally extensive salt detachment layer) showed a systematic northward increase from eastern Kentucky/West Virginia to eastern New York (his data could not reliably constrain $S_{H\max}$ magnitudes). He found that the northward increasing $S_{h\min}/S_v$ ratio could be modeled as the effect of persisting flexure stresses due to glacial rebound.

A number of analyses of glacial rebound-related stresses have been presented [e.g., *Stein et al.*, 1979, 1989; *Clark*, 1982; *Quinlan*, 1984; *James*, 1991]. In all models a reference or equilibrium state and a viscosity model are assumed, displacements in response to removal of the load are determined, and stresses and strains are computed from these displacements. Approximating the ice sheet as a circular load, rebound-related stresses can be represented as radial and tangential (relative to the center of the ice sheet near Hudson Bay) [e.g., *James and Morgan*, 1990]. In southeastern Canada and the northeastern United States the tangential stress due to rebound is subparallel to the regional ENE $S_{H\max}$ orientation, while the radial rebound stress is subparallel to $S_{h\min}$. In a two-dimensional analysis of rebound-related flexural stresses by *Clark* [1982], the ice sheet load was approximated as a right circular cylinder of paraboidal cross section with 5-km maximum thickness which was removed instantaneously. Vertical displacements were computed for a flat two-layer Earth model including a 100-km-thick elastic plate overlying an upper mantle of viscosity 10^{21} Pa s. His results indicate an increase in both radial and circumferential stress (relative to ambient or regional stress field) beneath the ice sheet load in southeastern Canada and a decrease in both radial and circumferential stress in front of the ice load in the central United States. His results therefore are qualitatively consistent with the observed contrast in relative stress magnitudes between the two areas,

and the predicted present-day values of flexural stresses are of the order of ±5 MPa for the radial stress values and ±1–2 MPa for the circumferential stress.

Using a more sophisticated five-layered spherical Earth model, *James* [1991] computed the approximate rebound-related change in stress magnitudes over the past 26,000 years for each of the three components (radial, tangential, and vertical which, as noted above, in the area of interest roughly coincide with $S_{h\min}$, $S_{H\max}$, and S_v). In the southeastern Canada/east central U.S. region (roughly 250 km north and south of the southern margin of the ice sheet), James found that (relative to a reference stress state at 26,000 years) the magnitude of the tangential rebound stress component is compressive and approximately constant across the region (between about 2.0 and 2.5 MPa), whereas rebound radial and vertical stress components vary across the region in an opposite sense and are of approximately the same magnitude (total change of 5 MPa in each across the region). The net affect of these changes is to increase the likelihood of thrust faulting beneath the formerly loaded region (decrease in S_v and increase $S_{h\min}$ magnitudes) and an increase in the likelihood of strike-slip faulting (decrease $S_{h\min}$ and increase S_v) in the region south of the ice sheet margin. The maximum lateral stress difference between $S_{h\min}$ and S_v predicted across the region approximate 250 km north and south of the ice sheet edge is about 10 MPa.

Despite very different methods of calculation, the total present-day stress effect of postglacial rebound appears capable of explaining stress differences of about 10 MPa between the thrust regime in southeastern Canada and the central eastern United States. It is interesting to note the contrast in the predicted stresses from the models of *Clark* [1982] and *James* [1991] which assume an unloaded preexisting state with the results of the often quoted simple one-dimensional glacial rebound model of *Stein et al.* [1979, 1989] which assumes that the unstressed equilibrium state of the lithosphere is glaciated. This latter model predicts horizontal extension in the previously glaciated region and horizontal compression outside of the ice sheet, with the superimposed stresses of the order of 10–15 MPa. However, the sense of the predicted superimposed stresses in the *Stein et al.* [1979, 1989] model are opposite to the contrast observed in southeastern Canada relative to the central eastern United States.

The rebound flexural stresses have been interpreted as sufficient to influence the stress field in the upper 1–2 km [*Clark*, 1982; *Evans*, 1989]. The potential perturbation at earthquake depths (typically 5–10 km in this region, Table 1) can be evaluated drawing on the analysis of frictional analysis presented above. Once again we assume that stress differences are determined by the strength of optimally oriented faults and also assume that in the seismically active zones pore pressures are somewhat elevated ($P_0 = 0.65S_v$). In this case, stress magnitudes at 7 km depth (average depth of earthquakes in this study across this region) can be calculated from equation (5) with $\mu_c = 0.65$, the vertical stress is taken as the lithostat, and approximate mean ϕ values are determined for the two stress regimes: $\phi = 0.25$ in the strike-slip case and $\phi = 0.40$ in the thrust faulting case. The stress magnitudes are shown in a Mohr's circle representation in Figure 8. It is clear that the difference in stress states between the two regions for this commonly assumed model of crustal stresses is greater than those predicted by

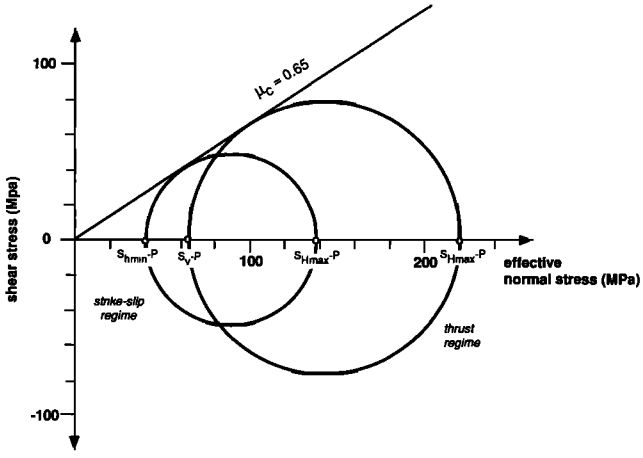

Fig. 8. Mohr's circle representation of predicted seismic zone stress magnitudes at 7 km depth for the thrust regime in southeastern Canada ($\phi = 0.4$) and the strike-slip regime in the central eastern United States ($\phi = 0.25$) determined using the frictional strength of optimally oriented faults with $\mu_c = 0.65$ and $P_0 = 0.65S_v$.

the rebound models (this is particularly true in terms of differences in $S_{H\max}$ magnitudes which *James* [1991] predicted should have very small changes, about 0.5 MPa, across this region).

Note too that knowledge of the ϕ values places valuable constraints on likely stress states. It can always be argued that if the stress regime is transitional between thrust and strike-slip faulting ($S_{h\min} \approx S_v$, corresponding to a $\phi = 0.0$ in both a strike-slip and thrust regime), then very minor perturbations in stress magnitudes could result in a difference in mechanism type between the two areas [e.g., *Talwani and Rajendran*, 1991]. However, the ϕ values for the southeastern Canada and central eastern U.S. region (CHV to SIL3) given in Figures 4*b* and 5*b* determined from the geometry of the slip vectors and regional stress field appear to rule out this possibility.

While the rebound-related stresses appear quite small and not capable of producing the stress regime changes shown in Figure 8, it is possible that stresses estimated from lithosphere strength assuming frictional strength values (with bulk frictional coefficients in the 0.6–0.85 range) may greatly overestimate the bulk strength of the upper brittle lithosphere. Considerable uncertainties remain regarding the magnitudes of in situ stress at seismogenic depths (see *Zoback* [this issue] for an alternate attempt to constrain stress magnitudes at depth using local horizontal stress rotations).

Furthermore, superimposed rebound-related stresses may not be the only force acting in the vicinity of the southeastern ice sheet margin to perturb the regional field. Compressive stresses related to support of a dense lower crustal structure beneath ancient intraplate rift zones appear large enough to perturb the modern day stress field in the vicinity of the Amazonas rift in Brazil [*Richardson and Zoback*, 1990; *Zoback*, this issue] and around the New Madrid rift [*Grana and Richardson*, 1991]. Possibly similar rift normal compressive stresses related to an ancient NE trending rift beneath the St. Lawrence seaway may act to increase $S_{h\min}$ magnitudes in southeastern Canada-northeastern U.S. border region, facilitating the change in stress regime.

CONCLUSIONS

Well-constrained focal mechanisms of 32 North American midplate earthquakes (m_b = 3.8–6.5) were evaluated to determine if slip is compatible with a broad-scale regional stress field derived from plate-driving forces and, if so, under what conditions (stress regime, pore pressure, and frictional coefficient). The earthquakes studied were the largest recent events in this region, and their focal mechanisms were generally constrained by both first motions and surface wave modeling. Using independent information on in situ stress orientations from well bore breakout and hydraulic fracturing data and assuming that this regional stress field has approximately horizontal and vertical planes (±10°) principal planes, the constraint that the slip vector represents the direction of maximum resolved shear stress on the fault plane was used to calculate a parameter defining the relative stress magnitudes, $\phi = (S_2 - S_3)/(S_1 - S_3)$, from the fault/stress geometry. As long as the focal mechanism has a component of oblique slip (i.e., the B axis does not coincide with the intermediate principal stress direction), this calculation identifies which of the two nodal planes is a geometrically possible slip plane [*Gephart*, 1985].

Slip in a majority of the earthquakes (25 of 32) was found to be geometrically compatible with reactivation of favorably oriented preexisting fault planes in response to the broad-scale uniform regional stress field. The ϕ calculation, using the assumption of a regional stress field with approximately horizontal and vertical principal planes, properly and uniquely identified the fault planes in four of the six earthquakes for which these planes had been moderately to well constrained (primarily based on aftershock distribution).

Slip in five events (StF1, StF2, SWM, CAR, WVA) was found to be clearly inconsistent with the regional stress field and appears to require a localized stress anomaly to explain the seismicity. Two of these events (StF1, StF2) were normal faulting earthquakes in the St. Francois Mountains, Missouri, with T axes orthogonal to one another. The remaining three (SWM, CAR, WVA) had oblique strike-slip mechanisms with P axes nearly 90° different than the regional trend. Significantly, all five of these events occurred prior to 1970 when regional networks were installed, and their focal mechanisms are inconsistent with more recent solutions of nearby smaller events. Two additional events from the New Madrid region (NM3 and NM4) have nodal planes striking within a few degrees of the inferred $S_{H\max}$ direction and may also record a local stress rotation within this active seismic zone; however, two other New Madrid have focal mechanisms consistent with the regional stress field and the two incompatible mechanisms were done prior to detailed velocity structure information in the New Madrid rift.

The likelihood of the geometrically possible slip on the selected fault planes was evaluated in the context of conventional frictional faulting theory. Since available in situ stress measurements sample only the upper 1–2 km in this region, the ratio of shear to normal stress on the fault planes at hypocentral depth was calculated relative to an assumed regional stress field. Regional stress magnitude were determined from (1) S_1/S_3 ratios based on the frictional strength of optimally oriented faults (the basis for the linear brittle portion of lithospheric strength profiles), (2) the computed relative stress magnitude (ϕ) values, and (3) a vertical principal stress assumed equal to the lithostat. Two end-member possibilities were examined to explain the observed slip in these less than optimally oriented fault planes. First, the frictional coefficient was held constant on all faults, hydrostatic pore pressure was assumed regionally, and the fault zone pore pressure was determined. Since pore pressure is a measurable quantity with real limits in the crust ($P_0 < S_3$), this end-member case was used to determine which of the geometrically possible slip planes were frictionally likely slip planes. Alternately, pore pressure was fixed at hydrostatic everywhere and the required relative lowered frictional coefficient of the fault zone was computed.

Slip in 23 of the 25 geometrically compatible earthquakes was determined to also be frictionally likely in response to an approximately horizontal and vertical regional stress field derived from plate-driving forces and whose magnitudes are constrained using by the frictional strength of optimally oriented faults (assuming hydrostatic pore pressure regionally). The conditions for slip on these 23 relatively "well-oriented" earthquake faults were determined relative to this regional crustal strength model and require only moderate increases in pore pressure (between about 0.4 and 0.8 of lithostatic, hydrostatic is about 0.37 of lithostatic) or, alternately, moderate lowering (<50%) of the frictional coefficient on the faults which slipped. Superlithostatic pore pressures are not required. Some combination of reduced friction and local pore pressure perturbations may also explain slip in these events.

Three additional focal mechanisms (McN, CHV, and Q-MH) that had slip vectors geometrically consistent with the regional stress field, however, required extremely low coefficients of friction (<0.3) or pore pressures far exceeding the least principal stress. These events may reflect either local stress rotations undetected with current sampling or poorly constrained focal mechanisms. An alternate mechanism available for the Q-M event, Q-MY, was frictionally compatible with a thrust faulting regime over the full uncertainty of stress orientations considered.

In the central and eastern United States, earthquakes occur primarily on strike-slip faults dipping between 43° and 80°, with most in the 60°–75° range. In contrast, slip in southeastern Canadian earthquakes occurs on faults dipping primarily 20°–50° which show dominantly thrust or reverse slip. A roughly north to south contrast in stress regime between the central eastern United States and southeastern Canada had been previously inferred from a contrast in focal mechanisms between the two areas [*Hasegawa et al.*, 1985; *Talwani and Rajendran*, 1991]. This analysis demonstrated that the central eastern U.S. earthquakes occur primarily in response to a strike-slip stress regime, whereas the southeastern Canadian events require a thrust faulting stress regime.

While the source of the orientation and general compressive nature of the regional stress field appears related to far-field plate-driving forces, this contrast in stress regimes requires a more local source of lateral variation of relative stress magnitudes. Superposition of stresses due to simple flexural models of glacial rebound stresses is of the correct sense to explain the observed lateral variation, but maximum computed rebound-related stress magnitude changes are quite small (about 10 MPa) and do not appear large enough to account for the stress regime change if commonly assumed

stress magnitudes determined from frictional strength apply to the crust at seismogenic depths. Additional lateral varying forces may also be acting in this region of midplate North America, such as compressive stresses related to support of a dense lower crustal structure beneath the ancient NE trending rift zones beneath the St. Lawrence seaway. Recognizing and constraining the magnitude of the source of these lateral stress variation will be critical in understanding the forces driving intraplate deformation and has important implications for assessing the likelihood of slip (seismic hazard) on identified geologic structures in this region.

Acknowledgments. This paper benefitted greatly from critical reviews of Steve Hickman, Pradeep Talwani, John Adams, Russ Wheeler, Keith Evans, Wayne Thatcher, and especially multiple reviews by Mark Zoback. Bob Herrmann provided helpful advice and additional background information on some of the focal mechanisms. Special thanks to Tom James for several useful discussions on glacial rebound stresses and for providing a copy of his recently completed Ph.D. thesis. The breakout studies in the central and eastern United States and much of the frictional faulting analysis presented were supported by the Nuclear Regulatory Commission. The paper was completed during a 1-year U.S. Geological Survey G. K. Gilbert Fellowship funded visit at Universitat Karlsruhe, Karlsruhe, Germany, which provided technical support.

REFERENCES

Adams, J., Canadian crustal stress database—A compilation to 1987, *Geol. Surv. Can. Open File Rep., 1622, 130 pp., 1987.*

Adams, J., Crustal stresses in eastern Canada, in Earthquakes at North Atlantic Passive Margins: Neotectonics and Postglacial Rebound, edited by S. Gregersen and P. W. Basham, pp. 355–370, Kluwer Academic, Boston, Mass., 1989.

Adams, J., and J. S. Bell, Crustal stresses in Canada, in *The Geology of North America*, Decade Map Vol. 1, *Neotectonics in North America*, edited by B. Slemmons et al., pp. 367–386, Geological Society of America, Boulder, Colo., 1991.

Anderson, E. M., *The Dynamics of Faulting and Dyke Formation With Applications to Britain*, 206 pp., Oliver and Boyd, Edinburgh, 1951.

Andrews, M. C., W. D. Mooney, and R. P. Meyer, The relocation of microearthquakes in the northern Mississippi embayment, *J. Geophys. Res., 90*, 10,223–10,236, 1985.

Angelier, J., Determination of the mean principal directions of stresses for a given fault population, *Tectonophysics, 56*, T17–T26, 1979.

Barosh, P. J., Neotectonic movement, earthquakes and stress state in the eastern United States, *Tectonophysics, 132*, 117–152, 1986.

Barton, C. A., M. D. Zoback, and K. L. Burns, In-situ stress orientation and magnitude at the Fenton Hill geothermal site, New Mexico, determined from wellbore breakouts, *Geophys. Res. Lett., 15*, 467–470, 1988.

Baumgartner, J., and M. D. Zoback, Interpretation of hydraulic fracturing pressure-time curves using interactive analysis methods, *Int. J. Rock Mech. Min. Sci., 26*, 461–470, 1989.

Bell, J. S., and E. A. Babcock, The stress regime of the western Canadian Basin and implications for hydrocarbon production, *Bull. Can. Pet. Geol., 34*, 364–378, 1986.

Bell, J. S., and D. I. Gough, Northeast-southwest compressive stress in Alberta: Evidence from oil wells, *Earth Planet. Sci. Lett., 45*, 475–482, 1979.

Bell, J. S., and D. I. Gough, The use of borehole breakouts in the study of crustal stress, in *Hydraulic Fracturing Stress Measurements*, edited by M. D. Zoback and B. C. Haimson, pp. 201–209, National Academy Press, Washington, D. C., 1983.

Bjarnason, I. T., and J. C. Pechmann, Contemporary tectonics of the Wasatch front region, Utah, from earthquake focal mechanisms, *Bull. Seismol. Soc. Am., 79*, 731–755, 1989.

Bott, M. H. P., The mechanics of oblique slip faulting, *Geol. Mag., 96*, 109–117, 1959.

Brace, W. F., and D.L. Kohlstedt, Limits on lithospheric stress imposed by laboratory experiments, *J. Geophys. Res., 85*, 6248–6252, 1980.

Byerlee, J. D., Friction of rock, *Pure Appl. Geophys., 116*, 615–626, 1978.

Carey-Gailhardis, E., and J. L. Mercier, A numerical method for determining the state of stress using focal mechanisms of earthquake populations: Application to Tibetan teleseisms and microseismicity of southern Peru, *Earth Planet. Sci. Lett., 82*, 165–179, 1987.

Choy, G. L., and J. Boatwright, Teleseismic and near-field analysis of the Nahanni earthquakes in the Northwest Territories, Canada, *Bull. Seismol. Soc. A.., 78*, 1627–1652, 1988.

Choy, G. L., J. Boatwright, J. W. Dewey, and S. A. Sipkin, A teleseismic analysis of the New Brunswick earthquake of January 9, 1982, *J. Geophys. Res., 88*, 2199–2212, 1983.

Clark, J. A., Glacial loading: A cause of natural fracturing and a control of the present stress state in regions of high Devonian shale gas, paper SPE 10798 presented at Unconventional Gas Recovery Symposium, Soc. of Pet. Eng., Pittsburgh, Pa., May 16–18, 1982.

Dart, R., Horizontal stress directions in the Denver and Illinois basins from the orientations of borehole breakouts, *U.S. Geol. Surv. Open File Rep., 85-733*, 41 pp. 1985.

Dart, R., South-central United States well-bore breakout data catalog, *U.S. Geol. Surv. Open File Rep., 87-405*, 95 pp., 1987.

Dart, R., and M. L. Zoback, Principal stress orientations on the Atlantic continental shelf inferred from the orientations of borehole elongations, *U.S. Geol. Surv. Open File Rep., 87-283*, 43 pp. 1987.

Dawers, N. H., and L. Seeber, Intraplate faults revealed in crystalline bedrock in the 1983 Goodnow and 1985 Ardsley epicentral areas, New York, *Tectonophysics, 186*, 115–131, 1991.

Evans, K. F., Appalachian stress study, 3, Regional scale stress variations and their relation to structure and contemporary tectonic, *J. Geophys. Res., 94*, 17, 619–17,645, 1989.

Gephart, J. W., Principal stress directions and the ambiguity in fault plane identification from focal mechanisms, *Bull. Seismol. Soc. Am., 75*, 621–625, 1985.

Goodacre, A. K., and H. S. Hasegawa, Gravitationally induced stresses at structural boundaries, *Can. J. Earth Sci., 17*, 1286–1291, 1980.

Grana, J. P., and R. M. Richardson, Finite element modeling of stress within the New Madrid seismic zone, *Eos Trans. AGU, 72*, 429, 1991.

Haimson, B. C., Crustal stress in the continental United States as derived from hydrofracturing tests, in *The Earth's Crust: Its Nature and Physical Properties, Geophys. Monogr. Ser.*, vol. 20, edited by J. C. Hancock, pp. 576–592, AGU, Washington, D. C., 1977.

Haimson, B. C., and T. W. Doe, State of stress, permeability, and fractures in the Precambrian granite of northern Illinois, *J. Geophys. Res., 88*, 7355–7372, 1983.

Haimson, B. C., and C. G. Herrick, In situ stress evaluation from borehole breakouts: experimental studies. *Proc. U.S. Symp. Rock Mech., 26th*, 1207–1218, 1985.

Hamilton, R. H., and M. D. Zoback, Tectonic features of the New Madrid seismic zone from seismic-reflection profiles, *U.S. Geol. Surv. Prof. Pap., 1236*, 31–38, 1982.

Harmsen, S. C., and A. M. Rogers, Inferences about the local stress field from focal mechanisms: Applications to earthquakes in the southern Great Basin of Nevada, *Bull. Seismol. Soc. Am., 76*, 1560–1572, 1986.

Hasegawa, H. S., Focal parameters of four Sverdrup Basin, Arctic Canada, earthquakes in November and December of 1972, *Can. J. Earth Sci., 14*, 2481–2494, 1977.

Hasegawa, H. S., and P. W. Basham, Spatial correlation between seismicity and postglacial rebound in eastern Canada, in *Earthquakes at North Atlantic Passive Margins: Neotectonics and Postglacial Rebound*, edited by S. Gregersen and P. W. Basham, pp. 483–500, Kluwer Academic, Boston, Mass., 1989.

Hasegawa, H. S., and R. J. Wetmiller, The Charlevoix earthquake of 19 August 1979 and its seismo-tectonic environment, *Earthquake Notes, 51*, 23–37, 1980.

Hasegawa, H. S., J. Adams, and K. Yamazaki, Upper crustal stresses and vertical stress migration in eastern Canada, *J. Geophys. Res., 90*, 3637–3648, 1985.

Hashizume, M., Surface wave study of earthquakes near northwestern Hudson Bay, Canada, *J. Geophys. Res.*, *79*, 5458–5468, 1974.

Herrmann, R. B., Surface-wave generation by the south central Illinois earthquake of November 9, 1968, *Bull. Seismol. Soc. Am.*, *63*, 2121–2134, 1973.

Herrmann, R. B., A seismological study of two Attica, New York earthquakes, *Bull. Seismol. Soc. Am.*, *68*, 1095–1102, 1978.

Herrmann, R., Surface wave focal mechanisms for eastern North American earthquakes with tectonic implications, *J. Geophys. Res.*, *84*, 3547–3552, 1979.

Herrmann, R. B., Surface-wave studies of some South Carolina earthquakes, *Bull. Seismol. Soc. Am.*, *76*, 111–121, 1986.

Herrmann, R. B., and J. Canas, Focal mechanism studies in the New Madrid seismic zone, *Bull. Seismol. Soc. Am.*, *68*, 1095–1102, 1978.

Herrmann, R. B., C. A. Langston, and J. E. Zollweg, The Sharpsburg, Kentucky, earthquake of 27 July, 1980, *Bull. Seismol. Soc. Am.*, *72*, 1219–1239, 1982.

Hickman, S. H., J. H. Healy, and M. D. Zoback, In situ stress, natural fracture distribution and borehole elongation in the Auburn geothermal well, Auburn, New York, *J. Geophys. Res.*, *90*, 5497–5512, 1985.

Hildebrand, T. G., M. F. Kane, and W. Stauder, Magnetic and gravity anomalies in the northern Mississippi Embayment and their relation to seismicity, *U.S. Geol. Surv. Misc. Field Study Map, MF-914*, 1977.

Horner, R. B., R. J. Wetmiller, and H. S. Hasegawa, The St. Donat, Quebec, earthquake sequence of February 18-23, 1978, *Can. J. Earth Sci.*, *16*, 1892–1898, 1979.

Jackson, J. A., Active normal faulting and crustal extension, *Geol. Soc. Spec. Publ. London*, *28*, 3–18, 1987.

Jaeger, J. C., and N. G. W. Cook, *Fundamentals of Rock Mechanics*, 3rd, 593 pp., Chapman and Hall, New York, 1979.

James, T. S., Post-glacial deformation, Ph.D. thesis, 190 pp., Princeton Univ., Princeton, N.J., 1991.

James, T. S., and W. J. Morgan, Horizontal motions due to post-glacial rebound, *Geophys. Res. Lett.*, *17*, 957–960, 1990.

Johnston, A., Seismicity of 'stable continental interiors', in *Earthquakes at North Atlantic Passive Margins: Neotectonics and Postglacial Rebound*, edited S. Gregersen and P. W. Basham, pp. 299–327, Kluwer Academic, 1989.

Johnston, A., and L. R. Kantor, Earthquakes in stable continental crust, *Sci Am.*, *262*, 68–75, 1990.

Kane, M. F., Correlation of major eastern earthquake centers with mafic/ultramafic basement masses, *U.S. Geol. Surv. Prof. Pap.*, *1028-O*, 199–204, 1977.

Lachenbruch, A. H., Frictional heating, fluid pressure, and the resistance to fault motion, *J. Geophys. Res.*, *85*, 6097–6112, 1980.

Langer, C. J., and G. A. Bollinger, The southeastern Illinois earthquake of 10 June 1987: The later aftershocks, *Bull. Seismol. Soc. Am.*, *81*, 423–445, 1991.

Mareschal, J.-C., and J. Kuang, Intraplate stresses and seismicity: The role of topography and density heterogeneities, *Tectonophysics*, *132*, 153–162, 1986.

Mitchell, B. J., Radiation pattern and attenuation of Rayleigh waves from the southeastern Missouri earthquake of October 21, 1965, *J. Geophys. Res.*, *78*, 886–899, 1973.

Mitchell, B. J., O. W. Nuttli, R. B. Herrmann, and W. Stauder, Seismotectonics of the central United States, in *The Geology of North America*, Decade Map Vol. 1, *Neotectonics of North America*, edited by B. Slemmons et al., pp. 245–260, Geological Society of America, Boulder, Colo., 1991.

Nabelek, J., and G. Suarez, The 1983 Goodnow earthquake in the central Adirondacks, NY: Rupture of a simple circular crack, *Bull. Seismol. Soc. Am.*, *79*, 1762–1777, 1989.

Nguyen, B. V., and R. B. Herrmann, Determination of source parameters for central and eastern North American earthquakes (1982–1986), *Seismol. Res. Lett.*, *62*, in press, 1992.

Nicholson, C., E. Roeloffs, and R. L. Wesson, The northeastern Ohio earthquake of 31 January 1986: Was it induced?, *Bull. Seismol. Soc. Am.*, *78*, 188–217, 1988.

North, R. G., R. J. Wetmiller, J. Adams, F. M. Anglin, H. S. Hasegawa, M. Lamontagne, R. Du Berger, L. Seeber, and J. Armbruster, Preliminary results from the November 25, 1988 Saguenay (Quebec) earthquake, *Seismol. Res. Lett.*, *60*, 89–93, 1989.

Paillet, F., and K. Kim, Character and distribution of borehole breakouts and their relationship to in situ stresses in deep Columbia River basalts, *J. Geophys. Res.*, *92*, 6223–6234, 1988.

Patton H., A note on the source mechanism of the southeastern Missouri earthquake of October 21, 1965, *J. Geophys. Res.*, *81*, 1483–1486, 1976.

Pine, R. J., P. Ledingham, and C. M. Merrifield, In situ stress measurements in the Carmenellis granite, II, Hydrofracture tersts at Rosemanowes Quarry to depths of 2000 m, *Int. J. Rock Mech. Min. Sci. Geomech. Abstr.*, *20*, 63–72, 1983.

Plumb, R. A., and J. W. Cox, Stress directions in eastern North America determined to 4.5 km from borehole elongation measurements, *J. Geophys. Res.*, *92*, 4805–4816, 1987.

Podrouzek, A. J., and J. S. Bell, Stress orientations from wellbore breakouts on the Scotian Shelf, eastern Canada, *Pap. Geol. Surv. Can.*, *85-1B*, 59–62, 1985.

Prowell, D. C., Index of faults of Cretaceous and Cenoaoic age in the eastern United States, *U.S. Geol. Surv. Misc. Field Stud. Map, MF-1269*, 1983.

Quinlan, G., Postglacial rebound and the focal mechanisms of eastern Canadian earthquakes, *Can. J. Earth Sci.*, *21*, 1018–1023, 1984.

Raleigh, C. B., J. H. Healy, and J. D. Bredehoeft, Faulting and crustal stress at Rangely, Colorado, in *Flow and Fracture of Rocks, Geophys. Monogr. Ser.*, vol. 16, edited by H. C. Heard et al., pp. 275–284, AGU, Washington, D.C., 1972.

Richardson, R. M., and L. Reding, North American plate dynamics, *J. Geophys. Res.*, *96*, 12,201–12,223, 1991.

Richardson, R. M., and M. L. Zoback, Amazonas rift: Modeling stress around a Paleozoic rift in South America, *Eos Trans. AGU*, *71*, 1606, 1990.

Rogers, G. C., R. M. Ellis, and H. S. Hasegawa, The McNaughton Lake earthquake of May 14, 1978, *Bull. Seismol. Soc. Am.*, *70*, 1771–1786, 1980.

Sbar, M. L., and L. R. Sykes, Contemporary compressive stress and seismicity in eastern North America: An example of intraplate tectonics, *Geol. Soc. Am. Bull.*, *84*, 1861–1882, 1973.

Schwartz, S. Y., and D. H. Christensen, The 12 July 1986 St. Mary's, Ohio earthquake and recent seismicity in the Anna, Ohio seismogenic zone, *Seismol. Res. Lett.*, *59*, 57–62, 1988.

Shamir, G., M. D. Zoback, and C. B. Barton, In situ stress orientation near the San Andreas fault: Preliminary results to 2.1 km depth from the Cajon Pass scientific drillhole, *Geophys. Res. Lett.*, *15*, 989–992, 1988.

Sibson, R. H., Frictional constraints on thrust, wrench and normal faults, *Nature*, *249*, 542–544, 1974.

Sibson, R. H., High-angle reverse faulting in northern New Brunswick, Canada, and its implications for fluid pressure levels, *J. Struct. Geol.*, *11*, 873–877, 1989*a*.

Sibson, R. H., Earthquake faulting as a structural process, *J. Struct. Geol.*, *11*, 1–14, 1989*b*.

Sibson, R. H., Rupture nucleation on unfavorably oriented faults, *Bull. Seismol. Soc. Am.*, *80*, 1580–1604, 1990.

Smith, R. B., W. C. Nagy, K. A. Julander, J. J. Viveiros, C. A. Barker, and D. C. Gants, Geophysical and tectonic framework of the eastern Basin and Range–Colorado Plateau–Rocky Mountain transition, *Mem. Geol. Soc. Am.*, *172*, 205–233, 1989.

Stein, S., N. H. Sleep, R. J. Geller, S.-C. Wang, and G. C. Kroeger, Earthquakes along the passive margin of eastern Canada, *Geophys. Res. Lett.*, *6*, 537–540, 1979.

Stein, S., S. Cloetingh, N. H. Sleep, and R. Wortel, Passive margin earthquakes, stresses and rheology, in *Earthquakes at North Atlantic Passive Margins: Neotectonics and Postglacial Rebound*, edited by S. Gregersen and P. W. Basham, pp. 231–259, Kluwer Academic, Boston, Mass., 1989.

Stock., J. M., and J. Healy, Stress field at Yucca Mountain, Nevada, *U.S. Geol. Surv. Bull.*, *1790*, 87–93, 1988.

Stock, J. M., J. Healy, S. H. Hickman, and M. D. Zoback, Hydraulic fracturing stress measurements at Yucca Mountain, Nevada, and relationship to the regional stress field, *J. Geophys. Res.*, *90*, 8691–8706, 1985.

Talwani, P., and K. Rajendran, Some seismological and geometric features of intraplate earthquakes, *Tectonophysics*, *186*, 19–41, 1991.

Taylor, K. B., R. B. Herrmann, M. W. Hamburger, G. L. Pavlis, A. Johnston, C. Langer, and C. Lam, The southeastern Illinois

earthquake of 10 June 1987, *Seismol. Res. Lett.*, *60*, 101–110, 1989.

Wetmiller, R. J., The Quebec-Maine border earthquake, 15 June 1973, *Can. J. Earth Sci.*, *12*, 1917–1928, 1975.

Wetmiller, R. J., J. Adams, F. M. Anglin, H. S. Hasegawa, and A. E. Stevens, Aftershock sequences of the 1982 Miramichi, New Brunswick, earthquakes, *Bull. Seismol. Soc. Am.*, *74*, 621–653, 1984.

Wetmiller, R. J., R. B. Horner, H. S. Hasegawa, R. G. North, M. Lamontagne, D. H. Weichert, and S. G. Evans, An analysis of the 1985 Nahanni earthquakes, *Bull. Seismol. Soc. Am.*, *78*, 590–616, 1988.

Yang, J.-P., and Y. P. Aggarwal, Seismotectonics of northeastern United States and adjacent Canada, *J. Geophys. Res.*, *86*, 4981–4998, 1981.

Zheng, Z., J. Kemeny, and N. G. W. Cook, Analysis of borehole breakouts, *J. Geophys Res.*, *94*, 7171–7182, 1989.

Zoback, M. D., and J. H. Healy, Friction, faulting and in situ stress, *Ann. Geophys.*, *2*, 689–698, 1984.

Zoback, M. D., and J. H. Healy, In situ stress measurements to 3.5 km depth in the Cajon Pass scientific research borehole: Implications for the mechanics of crustal faulting, *J. Geophys. Res.*, *97*, 5039–5057, 1992.

Zoback, M. D., and M. L. Zoback, Tectonic stress field of North America and relative plate motions, in *The Geology of North America*, Decade Map Vol. 1, *Neotectonics of North America*, edited by B. Slemmons et al., pp. 339–366, Geological Society of America, Boulder, Colo., 1991.

Zoback, M. D., R. M. Hamilton, A. J. Crone, D. P. Russ, F. A. McKeown, and S. R. Brockman, Recurrent intraplate tectonism in the New Madrid seismic zone, *Science*, *209*, 971–976, 1980.

Zoback, M. D., D. Moos, L. Mastin, and R. N. Anderson, Wellbore breakouts and in situ stress, *J. Geophys. Res.*, *90*, 5523–5530, 1985.

Zoback, M. D., W. H. Prescott, and S. W. Kroeger, Evidence for lower crustal ductile strain localization in southern New York, *Nature*, *317*, 705–707, 1985.

Zoback, M. D., et al., New evidence on the state of stress of the San Andreas fault system, *Science*, *238*, 1105–1111, 1987.

Zoback, M. L., State of stress and modern deformation of the northern Basin and Range province, *J. Geophys. Res.*, *94*, 7105–7128, 1989.

Zoback, M. L., First- and second-order patterns of stress in the lithosphere: The World Stress Map Project, *J. Geophys. Res.*, this issue.

Zoback, M. L., and M. D. Zoback, State of stress of the conterminous United States, *J. Geophys. Res.*, *85*, 6113–6156, 1980.

Zoback, M. L., and M. D. Zoback, Tectonic stress field of the conterminous United States, *Mem. Geol. Soc. Am.*, *172*, 523–539, 1989.

Zoback, M. L., S. P., Nishenko, R. M. Richardson, H. S. Hasegawa, and M. D. Zoback, Mid-plate stress, deformation, and seismicity, in *The Geology of North America*, vol. M, *The Western North Atlantic Region*, edited by P. R. Vogt and B. E. Tucholke, pp. 297–312, Geological Society of America, Boulder, Colo., 1986.

Zoback, M. L., et al., Global patterns of tectonic stress, *Nature*, *341*, 291–298, 1989.

M. L. Zoback, U.S. Geological Survey, 345 Middlefield Road, MS 977, Menlo Park, CA 94025.

(Received February 13, 1991;
accepted June 5, 1991.)